INSTITUTE OF PHYSICS PUBLISHING JOURNAL OF PHYSICS D: APPLIED PHYSICS

J. Phys. D: Appl. Phys. **38** (2005) R329–R355 doi:10.1088/0022-3727/38/21/R01

TOPICAL REVIEW

A review and outlook for an anomaly of scanning tunnelling microscopy (STM): superlattices on graphite

Wing-Tat Pong and Colm Durkan[1]

Nanoscience Centre, University of Cambridge, 11 J J Thomson Ave, Cambridge, CB3 0FF, UK

E-mail: cd229@eng.cam.ac.uk (C Durkan)

Received 4 March 2005
Published 24 October 2005
Online at stacks.iop.org/JPhysD/38/R329

Abstract

Since its invention in 1981, scanning tunnelling microscopy (STM) is well-known for its supreme imaging resolution enabling one to observe atomic-scale structures, which has led to the flourishing of nanoscience. As successful as it is, there still remain phenomena which are observed using STM but are beyond our understanding. Graphite is one of the surfaces which have been most extensively studied using STM. However, there are a number of unusual properties of graphite surfaces. First reported in the 1980s, superlattices on graphite have since been observed many times and by many groups, but as yet our understanding of this phenomenon is quite limited. Most of the observed superlattice phenomena are widely believed to be the result of a Moiré rotation pattern, arising from the misorientation between two graphite layers, as verified experimentally. A Moiré pattern is a lattice with larger periodicity resulting from the overlap of two lattices with smaller periodicities. As graphite layers are composed of hexagonal lattices with a periodicity of 0.246 nm, as observed using STM, when there are misoriented graphite layers overlapping each other, a Moiré pattern with larger periodicity, depending on the misorientation angle, will be produced and appear as a superperiodic hexagonal structure on top of the graphite atomic lattice of the topmost surface layer. It is important to study graphite superlattices because, firstly, knowledge of this phenomenon will enable us to properly interpret STM images; secondly, it helps us to understand the correlation between electronic structures and atomic-structure rearrangement of graphite which is of tremendous aid for engineering material properties; thirdly, and perhaps most importantly, the observation of the phenomenon exhibits the capability of STM to produce images indicating the nature of internal defects which are below the surface. Over recent years, experimental and modelling techniques have been developed to study this anomalous regime of STM; however, there is a lack of a systematic classification of this scattered information. This review article thus serves the purpose of organizing all these results so as to enable a more comprehensive understanding of this phenomenon. We review the discovery of graphite superlattices, the observation of the associated properties, and the research efforts on this subject. An effort is made to envision the future experimental and theoretical research possibilities to unveil the mystery of this anomaly of STM. Applications of graphite superlattices are also proposed.

(Some figures in this article are in colour only in the electronic version)

[1] Author to whom any correspondence should be addressed.

1. Introduction

1.1. Graphite as a common substrate for STM

Graphite is one of the most commonly used substrates in scanning tunnelling microscopy (STM). Having a Bernal-type structure with D_{6h}^4 symmetry, graphite consists of layers of sp^2 bonded carbon atoms [1], the layers being bound together by Van der Waals forces with ABAB stacking along the c axis. Upon cleavage, the surface comprises atomically flat terraces ranging in size from a few hundred nanometres to tens of micrometres and graphite surfaces are relatively chemically inert. Moreover, graphite can provide atomic resolution in STM even under ambient conditions and thus is the standard benchmark for STM performance. It has been extensively used as a substrate for deposition of chemical and biological species [2–15].

1.2. Graphite superlattices

Graphite superlattices have been observed by many groups over the last two decades (e.g. [16–24]). The subject of study here is superperiodic hexagonal structures on a graphite surface whose formation is due to intrinsic defects of the substrate crystal. They arise because dislocations occur during crystal growth or cleavage. Broadly speaking, there are four situations in which superperiodic structures can be observed. Firstly, it is well known that graphite forms intercalation compounds, for example with alkali-metals or electrolytic solutions, which show large-scale periodic superstructures, such as 2×2 and $\sqrt{3} \times \sqrt{3}$ superstructures. Secondly, there is a superlattice with a size of $\sqrt{3}$ times the graphite lattice constant observed using STM, the $\sqrt{3} \times \sqrt{3}\,\mathrm{R30}^\circ$ superstructure [25–33]. It is produced by the perturbation of the charge density by steps, point defects and grain boundaries. This structure is not a surface reconstruction where atoms are rearranged or removed from the surface. It is effectively similar to the Friedel oscillations in the charge density around an impurity, and moving away from the impurity will decrease the amplitude of the density modulation, and consequently this kind of $\sqrt{3} \times \sqrt{3}$ R30° superstructure is usually confined within a relatively small area of a few nanometres neighbouring a defect. Thirdly, superstructures can be due to adsorbed species on the graphite surface. Fourthly, superlattices may be observed if there is a misorientation of one or more of the graphite layers on or near the surface. In this paper, we will concentrate on the last kind of superlattice.

1.3. Significance of studying graphite superlattices

An STM image represents the electronic structure (local density of states (LDOS)) of a surface, which generally closely correlates with the geometric surface topography. However, in some cases, the STM image does not show the actual atomic arrangement at the surface. One typical example is graphite, where STM can only observe every second atom, i.e. the carbon atoms (β sites) on a graphite surface which do not have atoms directly below them. The origin of this phenomenon is the fact the other carbon atoms (α sites) have their electronic density of states at the Fermi level reduced by the atoms directly below them. Another example is the charge density waves observed on some low dimensional materials, such as TaS_2 and $NbSe_3$, resulting from an atomic displacement of a few tenths of an angstrom which induces patterns superimposed onto the atomic lattice in STM images [34–36]. It is important to understand how to interpret STM images; therefore the superlattices observed on graphite surfaces are an important subject to study as it is believed that a superlattice is a direct consequence of the interlayer electronic interaction of the topmost surface with the bulk, rather than an actual topographical feature. Such an electronic interference exhibits a potential problem for imaging deposited species on graphite, particularly if the deposited molecules form periodic structures on the graphite surface. Graphite is commonly used for deposition of various kinds of molecules or biological samples in STM experiments. In order to properly distinguish the presence of deposited materials on the graphite surface from the apparent modification in the atomic corrugation of graphite induced by the electronic interaction of the surface layer with the layers which are a few layers below, it is of paramount importance to understand the origin of the formation of graphite superlattices and the relationship between the superlattice pattern and the interlayer interaction. Another reason for studying graphite superlattices is their interesting electrical properties. The electronic properties of graphite are changed with the modification or intercalation of the basic AB-stacked Bernal structure, and as a consequence the electrical properties can be varied from those of an insulator to those of a superconductor [37]. As a superlattice involves the rotation of a graphite layer and modifies the graphite Bernal structure to include simple hexagonal and rhombohedral graphite structures, studies of superlattices will help us to understand the correlation between electronic structures and atomic-structure rearrangement of graphite which is of tremendous aid for engineering material properties. In this respect, STM studies on superlattices can provide information on the LDOS and atomic images to reveal such a correlation.

Perhaps the most intriguing and potentially useful aspect of graphite superlattices stems from the fact that the observation of a superlattice structure on a graphite surface indicates that STM, in addition to its capability to image the topmost surface, can potentially investigate the nature of internal defects which are in the bulk of the sample. This imaging capability of STM is not well studied. Our knowledge of superlattices will enable us to understand this aspect of STM functionality better.

1.4. The purpose of this review

This work is mainly motivated by the fact that graphite superlattices have not been fully understood and all the relevant research results have not been well catalogued. Most of the reports made so far have been on superlattices formed by chance during cleaving; however, not much follow-up work has been done to systematically investigate this intriguing phenomenon, mostly as there is no repeatable means of preparing a superlattice. This technical difficulty is an obstacle to carrying out thorough studies on superlattices.

This review paper is aimed at collecting, organizing and analysing the available documented information concerning

graphite superlattices together in a coherent, logical and critical way and presents them as an integrated single topic. In the following sections, we will review the observation of graphite superlattices using STM and provide an overview of this subject. In section 2, we will briefly introduce various kinds of defects observed on graphite using STM as defects are closely related to the occurrence of graphite superlattices. We then move on to talk about the experimental work leading to the discovery and observation of graphite superlattices. The proposed explanations including the Moiré rotation pattern assumption on the origin of graphite superlattices will be described and discussed. The experimental results which verified the validity of the Moiré rotation pattern hypothesis will be presented in section 2.4. As the Moiré rotation pattern hypothesis is widely accepted as the origin of graphite superlattices, symmetry of superlattices is explained on the basis of the Moiré assumption in section 2.5. After learning more about the origin and structure of a graphite superlattice, we will talk about how to study the graphite superlattice phenomenon theoretically by introducing a simulation model with its formulation and applications. Next properties of a graphite superlattice apart from its superperiodicity are discussed in section 2.7 so as to give a comprehensive understanding on the characteristics of a graphite superlattice. Readers will particularly see the relevance of the graphite defects described in section 2.1 in the preparation of a graphite superlattice in section 2.7.6. The Moiré pattern hypothesis, despite its wide acceptability, is challenged by the controversies brought about by some contradictory experimental and theoretical works which are included in section 2.8. Although the Moiré rotation pattern assumption enables us to understand the graphite superlattice phenomenon better, there are still some regimes of graphite superlattices remaining unexplained in this way. They will be mentioned in section 2.9. In section 3 we will first point out the research possibilities, both experimental and theoretical, on this subject to encourage more scientific endeavour on graphite superlattices. After that, we will talk about the possible applications of this interesting phenomenon on graphite. Finally, this paper ends with a conclusion.

2. Observation of graphite superlattice under STM

2.1. Large-scale features observed on graphite under STM

Graphite has been commonly used as a substrate in STM experiments since the invention of STM, as it offers many advantages for surface science research. However it does not come without drawbacks. Since 1990, there has been growing concern about various kinds of surface features associated with graphite. Although images illustrating the capability of STM to resolve the helicity of DNA have been presented [3, 38–40], Clemmer and Beebe discussed the ambiguities of graphite as a substrate for biological studies and reported the observation of regular periodicity from features that appear to meander across a freshly cleaved blank graphite surface [41]. Chang and Bard completed a comprehensive study on various kinds of surface features which are frequently observed upon cleavage of graphite [42]. Here we go through a brief review of graphite surface defects as they are closely related to the occurrence of superlattices; indeed, most superlattices are observed next to defects.

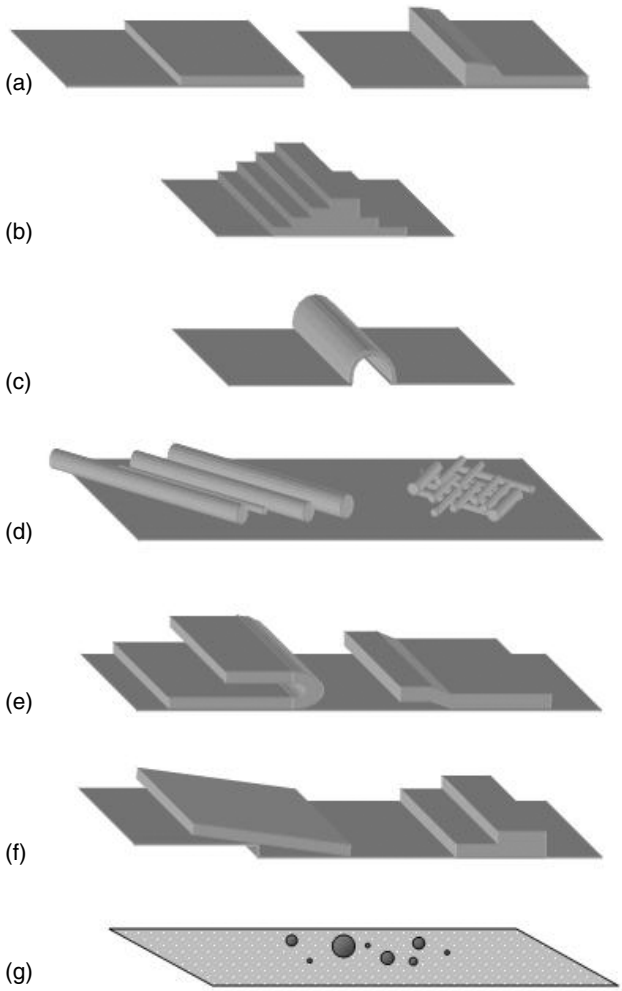

Figure 1. Schematic illustration of various kinds of surface defects observed on cleaved HOPG graphite. The categorization here follows the classification scheme proposed in [42]: (*a*) cleavage step; (*b*) ridge; (*c*) graphite strand; (*d*) fibres and fibre clusters; (*e*) folded-over flake and piece; (*f*) broken graphite pieces; (*g*) broken carbon particles.

Figure 1 shows a summary of the types of large-scale features often observed on graphite surfaces. The classification was done by Chang and Bard in 1991 [42]. Such a classification is not exhaustive as structures have been observed that cannot be classified into any of these categories. There are seven categories in all: (1) Cleavage steps (figure 1(*a*))—they can either be perfect steps (left of figure 1(*a*)) or distorted steps (right of figure 1(*a*)); (2) Ridges (figure 1(*b*)); (3) Graphite strands (figure 1(*c*)), which are often irregular in shape; (4) Graphite fibres and fibre clusters (figure 1(*d*)); (5) Folded-over flakes (figure 1(*e*)), pieces of graphite attaching to the cleavage steps where they originated. Superlattice structures due to Moiré rotation can often be observed on these folded-over flakes as there is usually a misorientation angle between the flake and the substrate. The folding over of graphite layers can be made use of in the preparation of a superlattice which will be discussed in section 2.7.6; (6) Broken pieces (figure 1(*f*)), graphite pieces completely detached from the

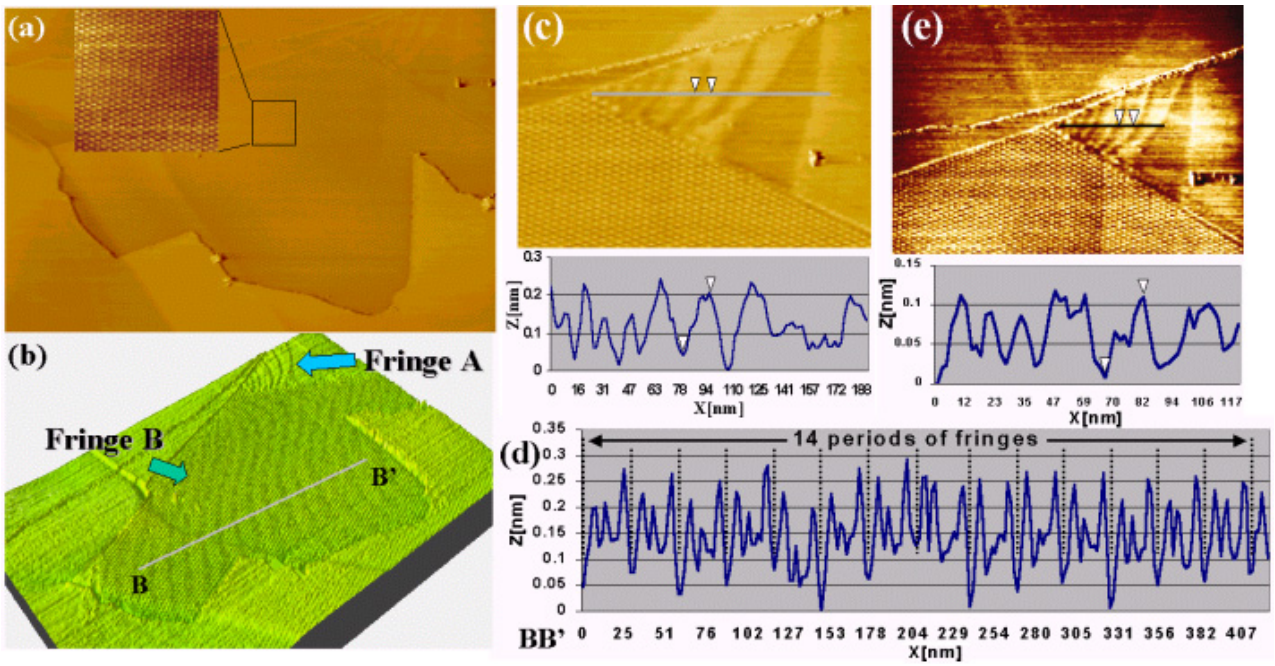

Figure 2. The rippling fringes on graphite from [43]. (*a*) 700 nm × 500 nm image ($I_t = 0.36$ nA, $V_s = 450$ mV) on graphite with the central part being the superlattice as shown by the inset. (*b*) Three-dimensional image of (*a*) with the contrast enhanced. The fringes at the corner and in the central part are labelled as fringe A and fringe B, respectively. The line profile BB′ is shown in (*d*). (*c*) 290 nm × 200 nm image ($I_t = 0.5$ nA, $V_s = 206$ mV) of fringe A in (*b*) with its cross-section. (*d*) Cross-section of fringe B along BB′ in (*b*). There are 14 periodicities of the rippling fringes shown in (*b*). The fringes are buried in the superlattice, and so the contrast has to be enhanced in order to display the rippling fringes in (*b*). (*e*) 400 nm × 350 nm image ($I_t = 0.36$ nA, $V_s = 450$ mV) of fringe A in (*b*) with its cross-section.

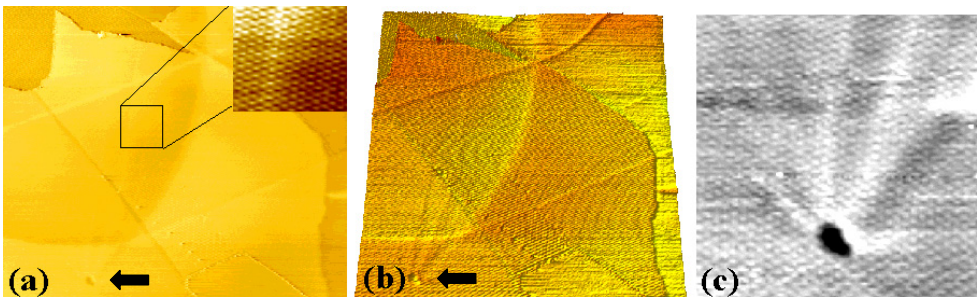

Figure 3. Another area with rippling fringes from [43]. (*a*) 800 nm × 750 nm image ($I_t = 0.5$ nA, $V_s = 206$ mV), with most of the area being a superlattice as shown by the inset. (*b*) Three-dimensional and contrast-enhanced image of (*a*), from where we can observe the rippling fringes again localized in the central part of the image. (*c*) The pit of monolayer depth associated with some long-ranged fringes which is positioned at the bottom left hand corner of (*a*) and (*b*) indicated by the arrows.

substrate and often in the form of a sheet; (7) Ultrasmall carbon particles (figure 1(*g*)), broken carbon pieces of the size of one to a small number of carbon atoms.

Another large-scale feature on graphite, related to superlattices and which has been reported recently [43], is that of one-dimensional fringes with periodicities of 20 and 30 nm and corrugations of 0.1 and 0.15 nm which have been observed on a superlattice (figures 2 and 3). The fringes were observed under differing tunnelling conditions as shown in figures 2(*c*) and (*e*). Moreover, the periodicities of the fringes are larger than that of the electronic wavelength on a planar graphite sheet, and therefore the fringes are unlikely to be an electronic standing wave on the surface. It is believed that these fringes reflect the actual surface topography of graphite along with the underlying superlattices and those nearby. This phenomenon is explained by the fact that there are many neighbouring superlattice regions with different periodicities and thus different rotation angles (according to the Moiré rotation pattern assumption). The net result is that these domains are rotating against each other. This generates a significant intralayer stress which causes the physical buckling of the surface as observed in the form of fringes using STM.

2.2. *Experimental procedures and results*

Most of the literature on graphite superlattices reports observations of freshly cleaved HOPG surfaces. As pointed out by Chang and Bard [42], HOPG surfaces cleaved by adhesive tape contain a larger coverage of defects than those cleaved by a razor blade. Since the occurrence of a superlattice is closely

related to defects, graphite surfaces cleaved with adhesive tape are more likely to exhibit superlattice structures. Mechanically cut Pt/Ir tips were commonly used in experiments, although there were a few exceptions in which etched gold tips [44], etched tungsten tips [31, 44–48], etched Pt/Ir tips [21, 49, 50], heteropolyacid (HPA)—functionalized Pt/Ir tips [51] and silicon tips [24] were used. Apparently the tip material does not affect the observed superlattice structures. The experiments were mostly conducted under ambient conditions, although some were under ultrahigh vacuum conditions [22, 48, 49, 52]; Oden *et al* [50] imaged graphite under triply distilled 18 MΩ water. Except for achieving atomic resolution on the underlying graphite atomic lattice, a constant current mode was generally used to image superlattices (except [45, 53], where a constant height mode was used). Various tunnelling conditions have been used, with bias voltages ranging from 10 to 650 mV and the tunnelling current from 0.09 to 5.6 nA. The periodicity of the observed superlattice structures ranges from 1.7 to 44 nm, with the corrugation from 0.5 to 20 Å. Table 1 is a list of the reported tunnelling conditions and the corresponding observed superlattices' periodicities and corrugations.

Figures 4(*a*) and (*b*) show typical superlattices observed on graphite using STM. In figure 4(*a*), the region to the right of the sharp boundary with a straight array of bright beads exhibits a hexagonal giant lattice with periodicity of 3.8 nm, a superlattice. The superlattice extends over an area of 500 nm × 500 nm. Superlattices generally measure a few hundred nanometres to a micrometre across [45]. A zoom-in of figure 4(*a*) is shown in figure 4(*c*), where the hexagon shows a unit cell of the superlattice. Superlattices have three-fold symmetry like the graphite atomic lattice, and in a superlattice unit cell, there are three brightest spots, three medium bright spots and one dark hole. Various kinds of notations are used to denote these different sites of a superlattice unit cell; for instance white spots, grey areas, dark areas [24]; peaks, valleys [20, 37]; g-β-site, g-α-site, g-h-site [24]. Despite such a variety, basically, in a superlattice unit cell, there are three levels of electron density of states, with three spots being the highest, three being medium and one being the lowest, which in fact is analogous to the graphite atomic lattice where a unit cell consists of three brightest β sites, three medium bright α sites and one dark hole site. The three-fold symmetry of superlattices will be discussed in section 2.5. Figure 4(*b*) is a closer view of the superlattice where the atomic resolution is shown. The orientation between the giant and atomic lattices is ∼28°, which agrees with the prediction by the Moiré pattern assumption for a superlattice with periodicity 3.8 nm. The relationship between the periodicity of a superlattice and its rotation angle and orientation will be delineated in section 2.3.6.

STM images of superlattices have been reported to be stable over a period of more than 30 h [20]. Also, superlattice structures have been observed to be independent of the variations in scan size (10–396 nm), scan rate (3.13–78.13 Hz) and image modes in the same experiment [21].

2.3. Proposed explanations on origin of superlattice

Superlattices on graphite are an intriguing phenomenon in STM, and some proposals have been made to explain their origin. The origin of superlattices is attributed to a network of dislocations, physical surface deformations, a multiple tip effect, adsorption of impurities, bond shortening, Moiré rotation patterns, and nanoscale defects at the subsurface. The Moiré rotation pattern assumption, supported by experimental evidence as discussed in section 2.4, is the most widely accepted explanation for superlattices on graphite.

2.3.1. Twist subboundary by a network of dislocations. Garbarz *et al* [19] interpreted the superlattice as the twist boundaries in the basal plane of graphite. They stated that the superlattice consists of a twist boundary which is formed by a 'honeycomb' network of dislocations, located in a basal plane a few angstroms below the surface. A model was proposed for this theory as shown in figure 5 which schematically shows the atomic displacement in a basal plane just above such a boundary. Dislocation splitting is not considered in this model. The dislocation segments of the honeycomb network have the Burgers vectors of the lattice constant ($b = 0.246$ nm) and have a screw orientation. The translation vectors d and the dislocation segments are perpendicular to each other in the dislocation network. The misorientation angle of the twist boundary can be found from $\theta \approx b/d$. Bernhardt *et al* [52] also attributed the appearance of a superlattice with non-constant periodicity observed on stressed graphite islands to the presence of a network of dislocations.

The evidence to support this explanation is their observation of a kink along the atomic row each time the row traverses from one bright superlattice spot (higher local density of states) to another, which agrees with their model of the honeycomb network of dislocations [19]. However, such a kink can also be explained by the odd–even transition theory proposed by Osing *et al* on a superlattice, based on the Moiré rotation assumption [22]. The theory states that when the Moiré rotation-pattern-induced superlattice is formed by one graphite monolayer, an atomic row should be wavy in pattern as it goes from one bright superlattice spot to another, and this theory is further supported by the simulation work in [54]. The odd–even transition theory will be further discussed in section 2.6.3.

2.3.2. Physical buckling of surface. It is intuitive to interpret STM superlattice structures as corrugations reflecting a physical buckling of the top graphite layer. A simple rigid-sphere intuition of graphite atoms inclines us to think that the interlayer spacing of AA-stacked graphite will be larger than that of AB-stacked graphite because it is appealing to perceive that the AA stacking of graphite will be repulsive as each atom on the first layer has another atom directly underneath it. Rong and Kuiper [23] have shown that this proposal does not fit. First of all, according to the *ab initio* calculation by Charlier *et al* [55], a hypothetical graphite with AA stacking has essentially the same interlayer spacing as AB-stacked graphite. The diffraction study of CAB-stacked orthorhombic graphite by Lipson and Stokes [56] also shows the same interlayer spacing. In addition, although rolling up a stiff sheet like graphite or paper does not require much energy, physically buckling a surface where the sheet is alternately expanded and compressed needs much more energy. In view of

Table 1. The tunnelling conditions used for imaging superlattices with STM reported in the literature with the corresponding observed superlattices' periodicities and corrugations.

Source of data	Bias voltage, V (mV)	Tunnelling current, I_t (nA)	Superlattice periodicity, D (Å)	Superlattice corrugation, ΔZ_s (Å)	Atomic corrugation, ΔZ_a (Å)
[22]	100	2	82	0.85 ± 0.15	1.2
[17]	500–650	0.8–3.5	35 ± 5	3 ± 0.4	—
[47]	150	—	50 ± 2	0.5	—
[86]	—	—	110	20	—
[87]	0.01	3	15	2	—
[43]	230	0.5	—	—	—
[43]	450	0.36	—	—	—
[43]	206	0.5	—	—	—
[71]	—	—	70.3	—	—
[72]	—	—	35	—	—
[72]	—	—	85	—	—
[44]	20	0.8	300	15	—
[44]	50	1	300	—	—
[44]	20	0.8	24	—	—
[44]	20	1.5	42	—	—
[19]	100	1	35	—	—
[23]	490	2.3	66	—	—
[23]	535	5	66	1[a]	0.4
[23]	72	5	66	2.6	0.6
[24]	−500 to +200	4.5	38[b]	12–14	2–3
[24]	−500 to +200	4.5	150[b]	1	—
[45]	33	0.4	60	—	—
[45]	30	0.26	117–124	—	—
[45]	43	0.19	117–124	—	—
[45]	50	1.2	117–124	—	—
[45]	80	0.35	117–124	—	—
[45]	4.9	0.4	96[a]	—	—
[49]	100	0.8	180–720	—	—
[20]	75	1	77 ± 2	10–15	—
[20]	102	1	77 ± 2	—	2 ± 1
[37]	125	1	36	0.6[c]	0.35
[37]	15	0.8	36	1.7	—
[37]	72	5.6	66	2.3	—
[37]	180	0.9	36	0.4[a]	—
[37]	20	0.8	36	1[a]	—
[48]	100	1	80	3.8	—
[48]	100	1	80	1.6[c]	—
[46]	150	1.1	105 ± 5	2.6 ± 0.1	0.36 ± 0.04
[52]	480	0.6	40 ± 1	—	—
[52]	210	0.6	40 ± 1	—	—
[52]	60	0.6	60–100	2–4[a]	—
[50]	100	1	148	2.1	—
[50]	100	1	105	2	—
[50]	100	1	50	5	—
[50]	100	1	440	5	—
[21]	20.1	2	44 ± 2	3.8 ± 0.2	—
[21]	178	2.4	44 ± 2	—	0.8
[80]	93	0.09	54 ± 1	1.4 ± 0.5	—
[18]	100	2	39±4	—	—
[16]	—	—	17.6	—	—
[16]	—	—	21.7	—	—
[53]	20	1.9	17.1	—	—
[53]	30	0.7	91	—	—
[76]	−50 to +100	0.5–5	31	—	—
[76]	−50 to +100	0.5–5	77	—	—
[76]	−50 to +100	0.5–5	59.5	—	—
[76]	−50 to +100	0.5–5	10.6	—	—
[76]	−50 to +100	0.5–5	12	—	—
[28]	—	—	$\sqrt{3} \times 2.46$	—	—
[31]	—	2	$\sqrt{3} \times 2.46$	—	—
[33]	3–160	1.5–14	1.5×2.46	—	—
[27]	48	3.2	$\sqrt{3} \times 2.46$	—	—
[25]	−300 to +300	0.1–0.5	$\sqrt{3} \times 2.46$	—	—
[26]	100	1	$\sqrt{3} \times 2.46$	—	—
[30]	100	1	$\sqrt{3} \times 2.46$	—	—

Table 1. (Continued)

Source of data	Bias voltage, V (mV)	Tunnelling current, I_t (nA)	Superlattice periodicity, D (Å)	Superlattice corrugation, ΔZ_s (Å)	Atomic corrugation, ΔZ_a (Å)
[32]	100	1	$\sqrt{3} \times 2.46$	—	—
[57]	50	1	101–760	—	—
[57]	150	1	60 ± 1	—	—
[57]	20.1	1	52 ± 2	—	—
[88]	−500 to +500	1	7.5	—	—
[89]	—	—	70×2.46	—	—
[90]	—	—	$\sqrt{3} \times 2.46$	—	—
[70]	1200	—	81	0.75	—
[70]	1200	—	81	0.35[c]	—
[70]	222	—	8.7	—	—
[70]	700	—	192[b]	—	—
[70]	700	—	32.5[b]	—	—
[70]	703	—	71	—	—
[70]	698	—	48	—	—
[70]	703	—	81	1.5	—
[70]	703	—	24	0.5	—
[70]	689	—	76	3	—
[70]	689	—	76	0.55	—
[70]	770	—	44	—	—
[91]	20	0.02	88	—	—
[91]	20	0.02	125	—	—
[92]	84	—	35	—	—
[93]	30	2	22	—	—
[51]	100	1.5	70.4	—	—
[51]	100	1.5	14.97	—	—

[a] Values measured from the figures, as they are not provided in the text.
[b] Superlattices superimpose with each other.
[c] Corrugation covered with one overlayer.

these, the corrugation of a superlattice is unlikely to represent the real atomic arrangement.

The first-principles calculation by Charlier *et al* [55] found the compressibility of bulk AAA graphite along the c axis to be six times lower than that of AB-stacked graphite. Thus a difference in the deformability of the different stacking structures can possibly explain superlattice structures. Nevertheless, the experimental result of Rong and Kuiper [23] disproved this possibility as the superlattice they observed had a corrugation of 2.6 Å and it was formed by a rotated graphite monolayer located 3.3 Å (very close to the ideal interlayer spacing of 3.35 Å, which means the deformation, if there is any, must be very small) above a common substrate and the deformability effect was much smaller than the superlattice corrugation.

2.3.3. Multiple tip effect. When the graphite superlattice was first observed in 1987, its origin was attributed to a multiple tip effect [16]. It was suggested that because of the microscopic roughness of the tip, two or more minitips may exist at the end of the tip, and when these minitips are very close or in contact with the surface, the repulsive forces arising from this contact will maintain these minitips at equal heights, and thereby the relative contribution of the tunnelling current from these minitips can be approximately the same. As such, the resulting STM image would be the superposition of the images from each minitip. If the multiple tips lie in more than one grain domain with different orientations of the atomic lattices simultaneously, the Moiré pattern would arise and result in the observed superlattice structure on the graphite surface under STM.

However, images having two domains showing both normal atomic resolution and long-range periodicities along the grain boundaries lie beyond the explanation given using the multiple tip effect model (figure 2(*a*) in [57]). It is rather improbable that two minitips resolving an atomic lattice contribute the same amount to the tunnelling current. In addition, this model fails to explain why such superlattice structures are not observed on other surfaces that contain grain boundaries.

2.3.4. Adsorption of impurities. In most cases the graphite samples were cleaved in air and the STM images were taken under ambient conditions, and so it is intuitive to conceive that some gas or liquid could be adsorbed onto the graphite surfaces, producing the superlattice structures. In the work of Kuwabara *et al* [20], both superlattice structure and underlying atomic lattice were imaged simultaneously, and this excluded the possibility that the superlattice they observed was due to adsorbed species. Also, superlattices have been observed under UHV conditions.

2.3.5. Dangling bonds at step edges leading to bond shortening. Buckley *et al* [45] suggested that the breakage of carbon–carbon bonds at step edges creates dangling bonds, where the valence electrons pair up and increase the double bond character of the surrounding carbon bonds. Since the double bond electrons are delocalized in graphite due to its conjugated structure, the increase in double bond character can spread over a large area and give rise to shortening of carbon–carbon bonds. In this way, some regions of the topmost layer

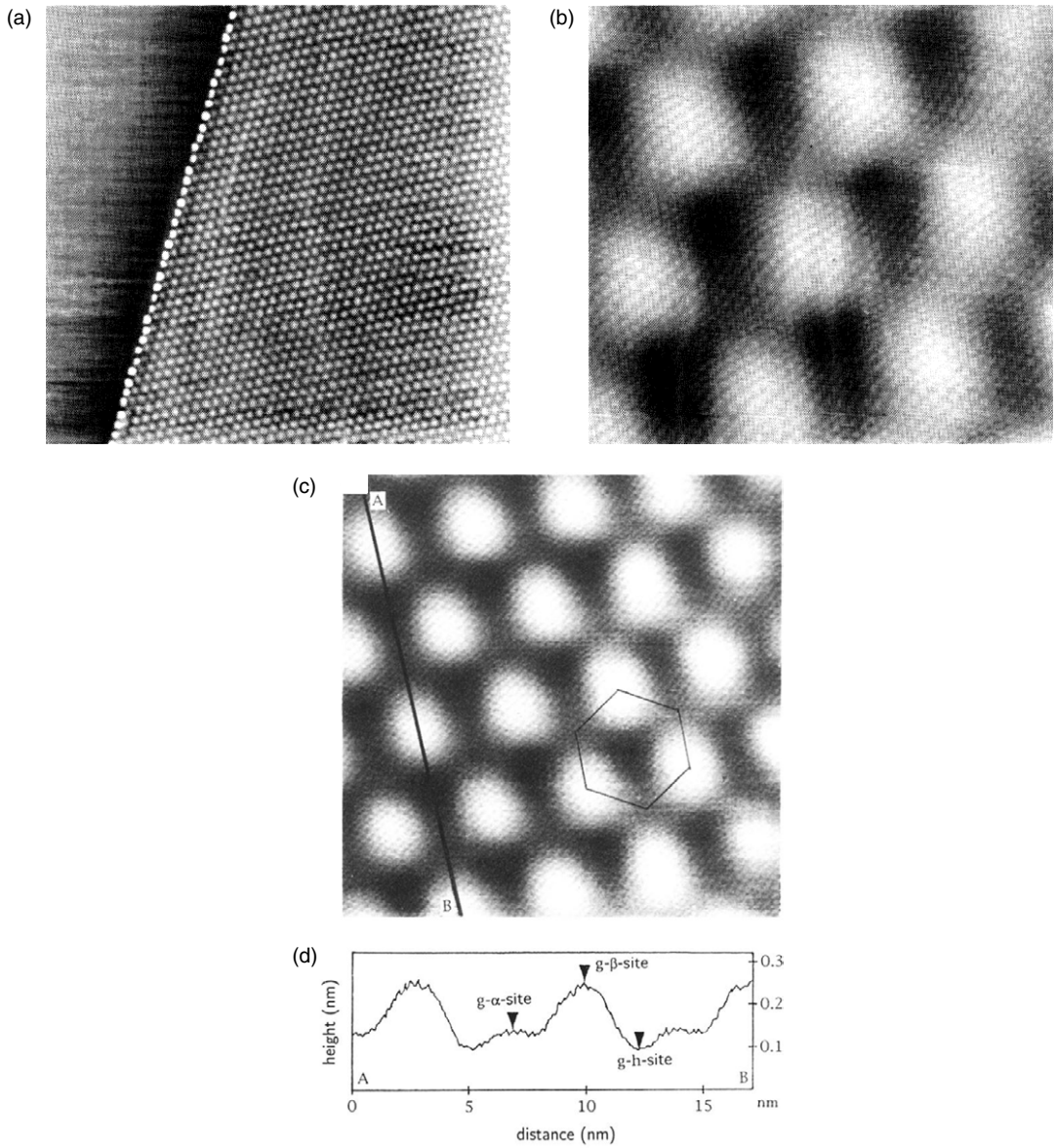

Figure 4. (*a*) 160 nm × 160 nm. On the left of the image, there is a sharp boundary separating the superlattice from the normal graphite. The superlattice on the right has a hexagonal symmetry with periodicity 3.8 nm. (*b*) 10 nm × 10 nm image which shows the superlattice and atomic lattice simultaneously. (*c*) An STM image (17 nm × 17 nm) on a graphite superlattice with a periodicity of 3.8 nm. The hexagon shows a unit cell of the superlattice. Similar to the graphite atomic lattice, there are three different sites with different heights (compared to the hole sites) in a superlattice unit cell. (*d*) A line profile along the line AB in (*c*). We can see that the g-β-site, g-α-site and g-h-site are of different heights, with the g-β-site being the brightest in the STM image. Images reprinted from [24] with permission from K Sattler.

could become reduced in size compared with the bulk graphite. This change in size can induce the Moiré pattern without rotational misorientation between graphite layers. Even a few per cent reduction in bond length could bring about large-scale periodicity as seen under STM. However, not much experimental evidence or theoretical work has followed to support this hypothesis.

2.3.6. Moiré rotation pattern assumption. Later Kuwabara *et al* and Liu *et al* proposed another explanation that the observed superperiodic structure is a rotational Moiré pattern resulting from the overlap between a misoriented layer of graphite and the graphite crystal underneath [20, 21]. The interlayer rotation is possibly caused by the cleavage step with a shear force or an epitaxial rotation in the growing process of graphite. The Moiré pattern [58, 59] assumption provides a good explanation for the observed periodicities of the superlattices in terms of the rotation angle between the graphite layers.

Moiré patterns, which are well-known from optics, are interference patterns resulting from rotation between two layers of any regular lattice (see [60] for a detailed description of Moiré patterns). When two layers of a lattice are rotated with respect to each other, interference occurs and it creates a superperiodic structure which shares the same symmetry as the original lattice on the two layers. This superperiodic structure is what is known as a superlattice. The periodicity of

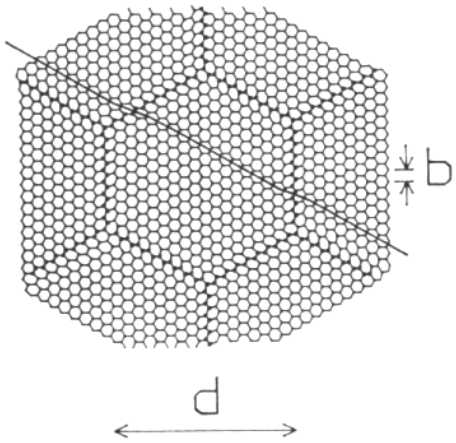

Figure 5. The honeycomb network of dislocations. The atomic displacement in a graphite layer close to a twist boundary is shown. The small hexagonal rings are the atomic lattice of graphite. The line traversing across the lattice indicates a kinked atomic row. (b) is a translation of the lattice and (d) is a translation of the dislocation network. Image reprinted from [19] with permission from E Lacaze and G Faivre.

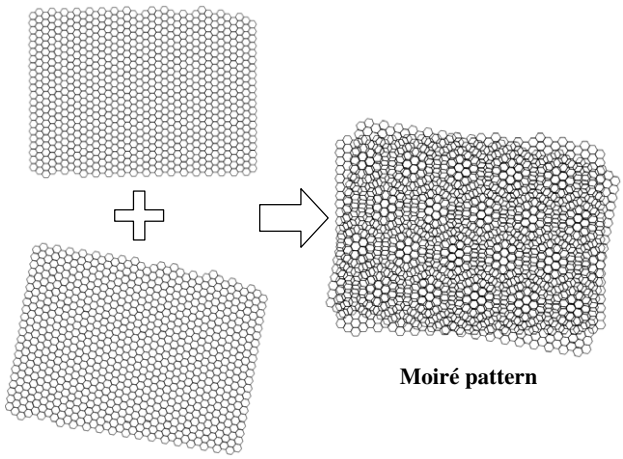

Figure 6. Visualization of Moiré pattern. There are two sets of hexagonal lattices with a misorientation angle of 10° between them; when they are overlapped together, another hexagonal lattice with larger periodicity appears, which is the resulting Moiré pattern.

this superlattice is dependent upon the rotation angle between the two original lattices. Figure 6 shows a Moiré pattern formed by overlapping of two lattices with identical hexagonal patterns and rotating them with respect to each other. The periodicity, D, of the resulting Moiré superperiodic hexagonal structure is related to the rotation angle, θ, between the two layers of the hexagonal lattice as

$$D = d/[2\sin(\theta/2)], \tag{1}$$

with d being the lattice constant of the smaller hexagonal lattice. The orientation of the Moiré pattern, ϕ, with respect to the atomic orientation of the top layer is related to the rotation angle, θ, as

$$\phi = 30^\circ - \theta/2. \tag{2}$$

2.3.7. Nanoscale defects a few layers below the surface. Using demonstrations by numerical calculations, Kobayashi proposed that, on the basis of three-dimensional tunnelling of STM, nanoscale electronic waves can propagate through many layers without decay because their lateral kinetic energy is smaller than the typical values of the Fermi energies; this means nanoscale structures can be observed using STM even if they are buried a few layers below the surface [61]. With this in mind, it is possible that a network of nanoscale defects in the subsurfaces can manifest itself on the topmost surface and modify the density of states, leading to the formation of a superlattice. No direct experimental proof has been reported in this respect so far. The corrugation conservation phenomenon reported in [43], which cannot be explained by the Moiré rotation pattern, may be an example of nanoscale waves propagating many layers without decay. Kobayashi also demonstrated numerically that when the tip–sample distance is short, only the atomic structure of the topmost layer is seen in STM images, and as the distance increases, the Moiré pattern becomes distinct. This simulated result is opposite to the experimental results of Osing and Shvets [22], who observed the superlattice when the tip was close to the surface, while only the graphite atomic lattice was imaged when the tip–sample distance was increased. This experimental result of Osing and Shvets will be discussed again in section 2.7.4.

2.4. Experimental results verifying the Moiré rotation pattern hypothesis

Kuwabara *et al* [20] worked out the relative orientation, ϕ, between the atomic lattice and the superimposed superlattice, and the periodicity, D, of the superlattice from STM images. Using equation (1), the rotation angle for a Moiré pattern to produce a superlattice with the periodicity D was calculated (with d being the graphite atomic lattice constant, 0.246 nm), which matches with the rotation angle found using equation (2) considering the relative orientation of the Moiré superlattice, ϕ. This is consistent with the Moiré rotation pattern assumption.

Rong and Kuiper [23] performed an experiment similar to that of Kuwabara. Rong and Kuiper looked at the rotation of the atomic corrugation in the superlattice region with respect to the exposed second layer and the normal graphite region next to the superlattice by imaging the surfaces with atomic resolution. This rotation angle was found to match the result calculated by substituting the periodicity of the superlattice, which can be measured from the STM image, and the already known graphite atomic lattice constant into the Moiré pattern equation (equation (1)). Moreover, the superlattice was found to be rotated about 30° with respect to the atomic lattice orientation, which agrees with the predicted orientation for a Moiré pattern given by equation (2).

In the experiment of Beyer *et al* [17] the topmost graphite monolayer was torn apart during the sample cleaving, and this layer folded back onto the substrate. By simultaneously imaging the part of the graphite covered by the rotated layer and the part not covered by such a layer, Beyer *et al* investigated whether the Moiré rotation pattern assumption is the correct explanation for a superlattice. Their results unambiguously show that only the overlapping area with a rotation angle between the two successive layers exhibited the superlattice structure, whereas the area not covered by the rotated layer

just showed the normal graphite lattice structure. The rotation angle, θ, between the two neighbouring layers was measured from the STM image and, knowing the atomic lattice constant, d, of graphite, the superlattice periodicity, D, was calculated and found to agree with that observed in the STM image. Gan *et al* [18] performed a similar experiment, but they used the tip to tear off the graphite layer and fold it back onto the substrate. The misorientation angle between this folded-back graphite layer and the substrate graphite crystal induced a superlattice with the periodicity as predicted by the Moiré rotation pattern assumption, again confirming the validity of the Moiré hypothesis.

These experimental results indicate that the Moiré rotation pattern assumption can successfully explain the origin of many of the superlattices observed on graphite.

2.5. Symmetry of superlattices (from the perspective of Moiré patterns)

Graphite superlattices have hexagonal symmetry, like the graphite atomic lattice in the sense that in a superlattice unit cell there are also three different sites; Xhie *et al* have provided elucidation on that [24]. Xhie *et al* used 'g-h-site', 'g-α-site', and 'g-β-site' as notations for the 'hole site' (darkest in STM superlattice images), 'α site' (second brightest) and 'β site' (brightest) in a superlattice, respectively, to avoid confusion with those in the atomic lattice (figure 4(d)).

The symmetry of the superlattice can be explained by considering the layered structure of graphite [24]. Graphite is normally made of ABAB... stacking, where alternate layers are laterally shifted by one nearest-neighbour distance, and carbon atoms in each layer are in the form of a honeycomb structure. The three-dimensional schematic drawing of the first three graphite layers is shown in figure 7(a). The shifting between alternate layers can be more easily seen from the plan view in figure 7(b). Every alternate atom on the top layer has an atom directly below, and these atoms on the top layer are notated as α sites, while the other atoms which do not have atoms directly underneath them are β sites. The graphite surface is composed of two hexagonal lattices: an α sublattice consisting of α sites; and a β sublattice consisting of β sites. Looking along the direction of the arrow in figure 7(b) will give the side view shown in figure 7(c). When a twist boundary occurs and the top layer is rotated, the original normal ABAB... stacking of graphite is distorted to CABAB..., where C is the notation for the rotated top layer. The misorientation between the top layer with stacking C and the second layer with stacking A induces a Moiré pattern which appears as the superlattice structure under the STM. By looking at the vertical alignment of the top layer atoms with the second layer atoms, we can categorize the atoms on the top layer into three groups. The model in [24] illustrates this categorization. Figure 7(d) shows the top C layer rotated 3.5° with respect to the underlying A layer. The large solid circles and the large dashed circles are of different kinds of regions with different atomic arrangements. In the large solid circles, each α atom in the A layer has an atom in the C layer directly or partially above it, whereas in the large dashed circles, each β atom has an atom in the C layer directly or partially above it. In this way, the sublattice contributed by the large solid circles and another sublattice established by the large dashed circles form the two hexagonal lattices, composing the large honeycomb structure of the Moiré pattern, which is similar to the graphite atomic structure where the structure is composed of the hexagonal lattice of α sites and the hexagonal lattice of β sites. The giant honeycomb in figure 7(d) is a unit cell of the Moiré pattern. The following notations for the honeycomb structure are used: 'M-α-sites' for the centres of the large dashed circles; 'M-β-sites' for the centres of the large solid circles and 'M-h-sites' for the centre of the giant honeycomb. This is the reason for the Moiré pattern displaying a hexagonal symmetry with three different sites in a unit cell. This symmetry comes from the difference between the α and β sites of the second layer, and this explains the similarity between the atomic structure and the superlattice structure of graphite.

Xhie *et al* also suggested an explanation for the coexistence of the atomic lattice and the superlattice. Despite the fact that every atom on a graphite surface is essentially identical, the atoms (β sites) which sit above the holes in the second layer appear at a higher intensity in STM images than do the atoms (α sites) which sit above the atoms in the second layer. Therefore, the atomic spacing for graphite under the STM is 0.246 nm rather than the actual 0.142 nm as the STM is imaging every other atom, and therefore the six-fold symmetry of the carbon rings appears as three-fold symmetry under the STM. Such an asymmetry arises because of the ABAB... stacking of the graphite layers which leads to the distinction between the α sites and β sites. The electronic interlayer interaction creates a band overlap and moves the wavefunctions of the α atoms away from the Fermi energy. Since the STM is imaging at the small energy range around the Fermi level, the β atoms are much more noticeable in the STM images. This is the situation for the normal graphite ABAB stacking. The atomic arrangement becomes more complex when the top layer is rotated; that is the stacking changes from ABAB... to CABAB.... An atom in the top layer can be above any site in the second layer, an α site, a β site, or a hole site or anywhere in between these locations. Although not proven by theoretical calculation, by using a reason similar to that for the intensity difference between the α atoms and β atoms for normal ABAB... stacking, Xhie *et al* proposed that an atom in the top rotated layer above a hole site in the second layer would show maximum intensity in the STM images just like β atoms in a normal graphite lattice with normal stacking. Likewise, an atom above an α atom in the second layer would show a lower intensity and an atom above a β atom would show the minimum intensity. With that assumption in mind, we then look at the atomic arrangement inside 'M-α-sites', 'M-β-sites' and 'M-h-sites'. In an M-h-site, atoms in the top layer are either covering an α site or β site in the second layer, and those above the α sites will be brighter in the STM images and constitute a hexagonal lattice. In an M-α-site (M-β-site), atoms in the top layer are either above hole sites in the second layer or above β sites (α sites), and the atoms above the hole sites will be brighter in the STM images and appear as a hexagonal lattice. In this way, the hexagonal atomic lattice is maintained throughout the surface even in the presence of the Moiré induced superlattice structure. The M-β-sites of the Moiré pattern should appear the brightest as the atoms of the M-β-sites are above either the

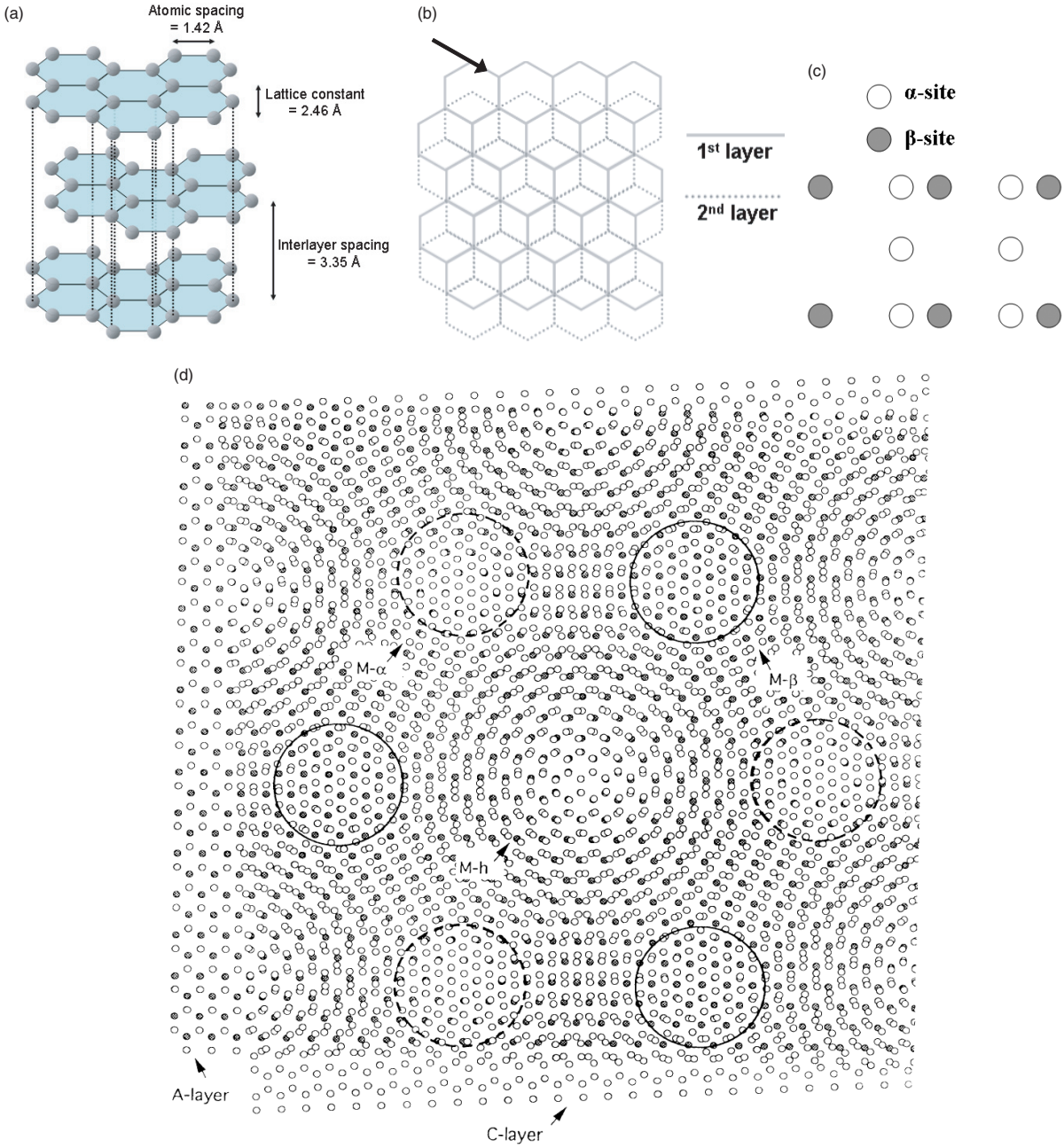

Figure 7. (*a*) A schematic drawing for three layers of graphite. (*b*) The plan view of the two neighbouring layers of graphite. (*c*) The side view of the layered structure of graphite along the arrow in (*b*). (*d*) The model of the Moiré pattern proposed by Xhie *et al* [24]. Two layers of the hexagonal atomic lattice are overlapped together with a misorientation angle of 3.5°. Image reprinted from [24] with permission from K Sattler.

hole sites or α sites in the second layer, which will render the atoms of the M-β-sites a higher electronic density of states. Likewise the M-α-sites are expected to be the second brightest, while the M-h-sites are the darkest in the STM images. Following this analysis, M-β (g-β)-sites should be the peaks of the superlattice; M-α (g-α)-sites should be the valleys of the superlattice; M-h (g-h)-sites should be the holes of the superlattice. The model proposed by Xhie *et al* can explain the three sites with different brightness in a superlattice and the coexistence of the superlattice and the atomic lattice; however, theoretical calculation would be necessary to further confirm its validity. The above analysis is based on the model in figure 7(*d*) whose misorientation angle is 3.5°; models with other misorientation angles should also be tried out in order to verify the above analysis.

The model of Xhie *et al* is based on the surface–atom location relative to normal AB-stacked graphite crystal underneath: atoms above hole sites give the highest density of states, atoms above α sites give the second-highest density and atoms above β sites give the lowest. However, Rong and Kuiper [23] performed the assignment of local stacking by considering the local crystal structure of the topmost layers from the perspective of the band-structure calculation by Charlier *et al* [62]. The difference between models of

Xhie *et al* and Rong and Kuiper will be further discussed in section 2.8.3.

2.6. Simulation model for investigating superlattice

2.6.1. Introduction. Graphite with a rotated layer is more complex for analytical analysis because upon rotation of a graphite layer an atom of the rotated layer can find itself above an α site, β site or hole site or somewhere in-between in the neighbouring layer, and thus it is difficult to determine the intensity of each atom on the rotated layer in STM images. Moreover, it is impossible to deliberately prepare a specific superlattice structure for STM experiments.

In light of the above, Cee *et al* [63] made use of a formula, first applied in molecular dynamic simulations, describing a continuous hexagonal lattice similar to that of graphite [64], to simulate graphite layers. Based on the Moiré rotation pattern model proposed by Xhie *et al* [24], Cee *et al* established the superlattice simulation model with the principle that an atom above an α site must be brighter than an atom above a β site in STM images. This simulation model can generate a superlattice with periodicity corresponding to the parameter of a rotation angle, which can qualitatively account for an observed superlattice.

2.6.2. Formulation. The electronic density of states of a layer n, Φ_n, at a position (x, y) is

$$\Phi_n = 1 - \frac{2}{9}\left[\cos\left[\left(\frac{2\pi}{2.46}\right)\left(x'' + \frac{y''}{\sqrt{3}}\right)\right] + \cos\left[\left(\frac{2\pi}{2.46}\right)\left(x'' - \frac{y''}{\sqrt{3}}\right)\right] + \cos\left[\left(\frac{4\pi}{2.46}\right)\left(\frac{y''}{\sqrt{3}}\right)\right] + \frac{3}{2}\right]. \quad (3)$$

In equation (3), there are three key components corresponding to the three vectors describing the hexagonal lattice and pointing to three different directions which are 120° separated from each other, with a periodicity of 2.46 Å to simulate the varying atomic density of a graphite layer. A detailed explanation of this formula can be found in [54]. More than one layer needs to be modelled in order to simulate a layered structure of Bernal graphite. However, for the Bernal structure there is a relative shift between the alternating layers, and therefore we need to modify x, y in equations (4) and (5) so that every other layer is shifted by 1.42 Å. To simulate a Moiré-rotation-induced superlattice, equations (6) and (7) are used to integrate the rotation angle into the model by rotating the coordinates with an angle θ.

$$x' = x + \Delta x = x + 1.42 \times \cos 30^\circ, \quad (4)$$

$$y' = y + \Delta y = y + 1.42 \times \sin 30^\circ, \quad (5)$$

$$x'' = x' \cos\theta - y' \sin\theta, \quad (6)$$

$$y'' = x' \sin\theta + y' \cos\theta. \quad (7)$$

2.6.3. Applications. This simulation model is a useful tool for investigating superlattice-related phenomena. First of all, it can simulate superlattices with various rotation angles, with the rotation taking place on any of the three layers. Some other interesting features of superlattices including odd–even transition of atomic rows [22], a superlattice with a screw dislocation [49], and twist and glide boundaries [48], can be analysed with the aid of this model as will be discussed in this section.

Construction of superlattice model. A Moiré rotation-pattern-induced superlattice arises from rotation between two graphite layers, and thus a superlattice can be simulated as two graphite layers with a misorientation angle between them. Simulations of STM images on graphite generally include the effect of a third layer underneath the first two. Weighting for each layer is as per the contribution of each layer to the overall structure. In normal cases, 1, 0.5 and 0.125 (normal weightings) are used for the first, second and third layers, respectively, based on the assumption that the influence of a layer should decay with its depth from the surface [48]. By adding the atomic density contribution of each layer together, an STM image can be simulated with the intensity, I, at a point (x, y) as:

$$I(x, y) = \Phi_1(x, y) - W_2\Phi_2(x, y) + W_3\Phi_3(x, y), \quad (8)$$

where Φ_n is the atomic density of layer n, and W_2 and W_3 are the weightings reflecting the relative contribution of the second and third layers. Figures 8(*a*) and (*b*) show a 20 nm × 20 nm superlattice area simulated with a rotation angle of the first layer of 2.5°, $W_2 = 0.5$ and $W_3 = 0.125$. The three-fold symmetry of a superlattice is shown as observed under STM.

Odd–even transition. Osing and Shvets [22] proposed that when the formation of a superlattice is due to only one rotated layer, there must be a shift along an atomic row as it traverses across a superlattice maximum, and thus the whole atomic row will look wavy and not straight. Such a phenomenon is named an odd–even transition, and it is confirmed by the simulation model [54] that when there are two rotated layers, the 'odd–even' transition will not be exhibited, whereas the transition phenomenon will be manifested if there is only one rotated layer (see figures 9(*a*) and (*b*)). The influence of the periodicity of a superlattice on its 'odd–even' transition phenomenon was explored, and it is found that as the periodicity of the superlattice increases, the transition will be less significant due to the fact that the transition occurs over a longer distance and thus gets smeared out (see figures 9(*b*)–(*d*)).

Superlattice with screw dislocation. Superlattices generally have constant periodicities and their patterns remain the same over the whole region. However, Feddes *et al* [49] observed a superlattice with its periodicity varying around a screw dislocation (figure 10(*a*)). The periodicity of the superlattice varies from 18 to 72 nm around the screw dislocation. Feddes *et al* used a different model which is based on an idea similar to that of equation (3), but it is slightly different in the way that the model uses two conditions to rule out non-physical phenomena: first, the atomic density is not allowed to increase as a result of interlayer interactions; second, the

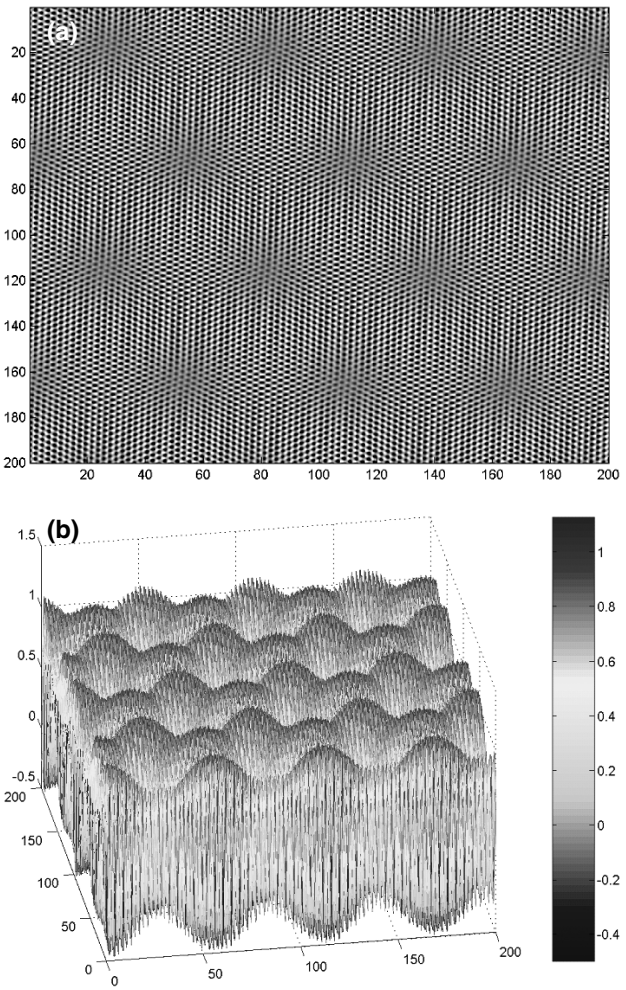

Figure 8. (*a*) The two-dimensional image of the 20 nm × 20 nm superlattice with a rotation angle of 2.5° (periodicity 5.64 nm) is simulated with $W_2 = 0.5$ and $W_3 = 0.125$. The bright area is higher than the dark area. (*b*) The three-dimensional image of the 20 nm × 20 nm superlattice in (*a*). The three-fold symmetry is obvious in (*b*), where the height difference between alternating peaks is discernible.

simulated density cannot become smaller than the minimum value of the first layer. These are achieved by adjusting a cut-off parameter of the second layer and a scaling parameter for controlling the subtraction of the second layer atomic density from the first layer. In the Feddes *et al* model, the simulated atomic density of a layer at any point (x, y) is

$$p(x, y) = \delta(x, y) + \delta(x, y - 1.23), \tag{9}$$

in which

$$\delta(x, y) = \cos\left[\left(\frac{2\pi}{2.46}\right)\left(x + \frac{y}{\sqrt{3}}\right)\right] + \cos\left[\left(\frac{2\pi}{2.46}\right)\left(x - \frac{y}{\sqrt{3}}\right)\right] + \cos\left[\left(\frac{4\pi}{2.46}\right)\left(\frac{y}{\sqrt{3}}\right)\right]. \tag{10}$$

the first component in equation (9) describes the α sites, while the second component describes the β sites. In this way, the physical significance of α or β sites can be individually adjusted so that the simulated image matches the usual STM image of graphite surfaces. Readers are referred to [49] for details of the Feddes model. Feddes *et al* simulated a superlattice with its rotation angle (and thus its periodicity (from equation (1), varies around the screw dislocation (figure 10(*b*)). As such, it was shown that the anomalous phenomenon of the superlattice around a screw dislocation is likely to be due to the varying rotation angle of the graphite layer around the screw dislocation. Bernhardt *et al* [52] and Sawamura *et al* [57] also observed superlattice structures with varying periodicities. However, the variations were along one direction rather than circulated around a screw dislocation.

Twist and glide boundaries. Sun *et al* [48] used a simulation model to investigate the twist boundary between two different regions of superlattices. They constructed a Moiré pattern using three layers, and along one close-packed direction the image is divided into halves with different stacking faults. In this way, the simulated image is in agreement with the observed STM image, indicating that the boundary is indeed a twist boundary. The boundary with two parallel rows of bright protrusions between two different superlattice regions was studied by dividing the image along one close-packed direction into halves, with the other half glided along the 30°/60° direction with different gliding distances, which are an integral number of times the superlattice periodicity and fractional periodicity (1/3 for 30°, 1/2 for 60°). The simulation results showed that the boundary is a glide boundary, and by comparing the simulation results of the twist and glide boundaries, Sun *et al* concluded that it is insufficient to identify twisting from gliding only based on a symmetry consideration.

Integrating tip shape and tip–sample distance. It is possible to take the tip shape and the tip–sample distance into consideration and integrate them with the simulation model. First used by Sawamura *et al* [57] in the three-dimensional simulation for the experimental STM image on the superlattice based on the rotation angle of the crystal axis of the tip with respect to the substrate crystal axis, this equation (equation (11)) defines the tunnelling current as the summation of currents due to tunnelling from each atom on the tip to every atom of the sample surface. The current intensity between an atom on the surface and an atom at the tip is described by the Tersoff and Hamann relation in the low bias limit [65]. The net tunnelling current from an STM tip located at the position (l, k) to the surface can be defined as:

$$I_{\text{total}} = \sum_i \sum_j I_{ij}(l, k), \tag{11}$$

in which

$$I_{ij}(l, k) = A \exp[-\alpha\{(x_{ij} - x_{lk})^2 + (y_{ij} - y_{lk})^2 + (z_{ij} - z_{lk})^2\}^{1/2}], \tag{12}$$

where $I_{ij}(l, k)$ is the tunnelling current between an atom at (x_{ij}, y_{ij}, z_{ij}) on the surface and an atom at (x_{lk}, y_{lk}, z_{lk}) at the STM tip, and α is dependent upon the characteristics of the materials of both the tip and surface.

By integrating this formulation into the simulation model, we can first simulate the graphite lattice using equation (3), and then consider the shape of the tip and the tip–sample distance

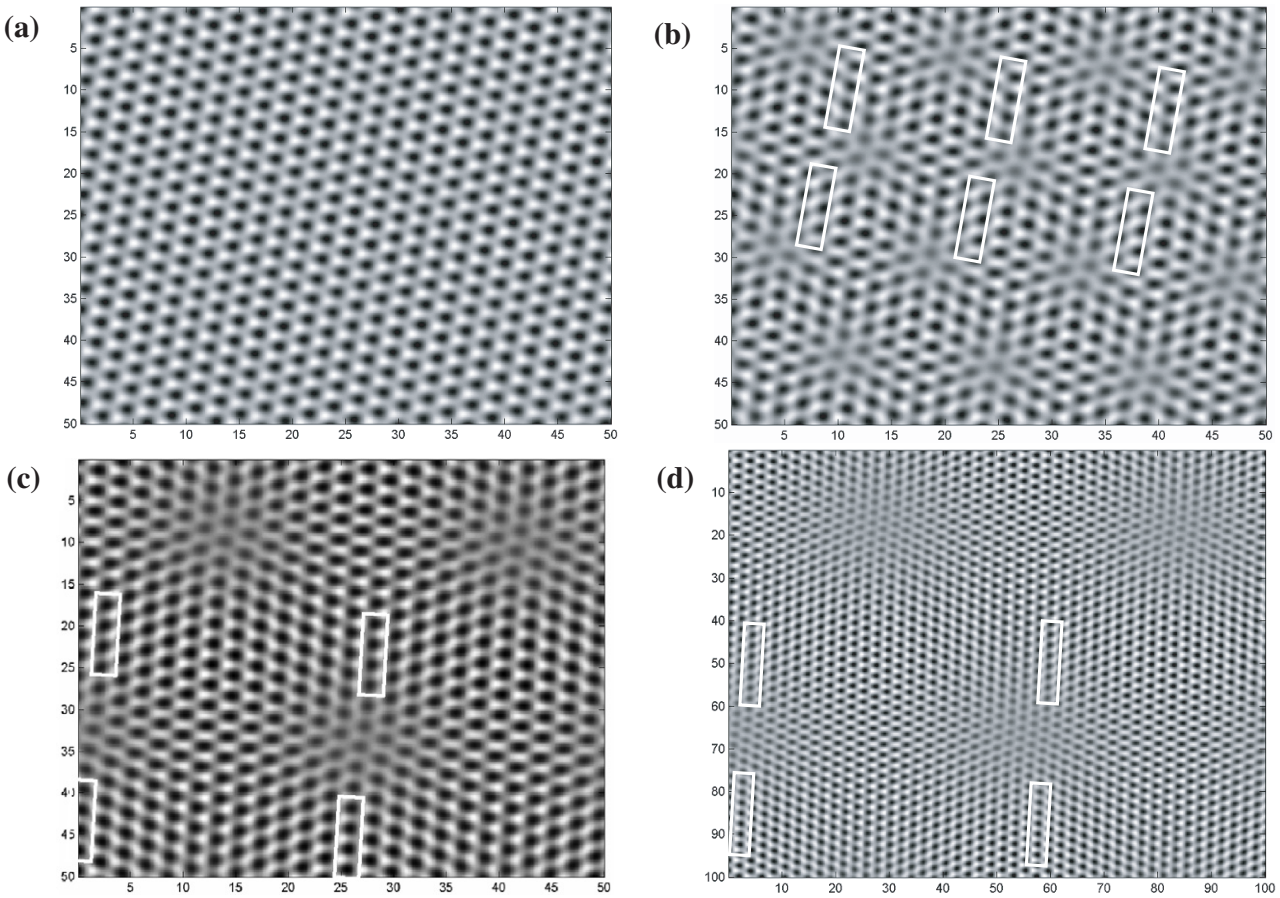

Figure 9. 'Odd–even' transition phenomenon on superlattice. (*a*) 5 nm^2 superlattice area with first and second layers rotated by 10° relative to the third layer and a periodicity of 1.41 nm. (*b*) 5 nm^2 superlattice area with first layer rotated by 10° relative to the second and third layers and a periodicity of 1.41 nm. (*c*) 5 nm^2 superlattice area with first layer rotated by 5° relative to the second and third layers and a periodicity of 2.82 nm. (*d*) 10 nm^2 superlattice area with first layer rotated by 2.5° relative to the second and third layers and a periodicity of 5.64 nm. All images are simulated with the normal weightings of $W_2 = 0.5$ and $W_3 = 0.125$. The proposal of the 'odd–even' transition by Osing and Shvets [22] is proven by the simulation results shown in (*a*) and (*b*), where only (*b*) shows the transition. As the periodicity increases from (*b*) to (*d*), the transition phenomenon gets smeared out over distance.

using equations (11) and (12). The final simulated STM image will be the image of the net tunnelling current which is the summation of all tunnelling occurrences between the tip and the sample.

2.7. *Other properties of superlattices*

2.7.1. Transition by high bias and tip–sample interaction. Since graphite layers are held together by weak Van der Waals forces, it is relatively easy to induce transitions of dislocation structures on a graphite surface by varying the bias voltage of the STM. Also, the superlattice structure can be damaged by scanning with a high bias. Buckley *et al* demonstrated that by scanning with a bias of 3 V in constant height mode, a 20 nm × 60 nm superlattice area was completely disrupted, and repeated scanning at 50 mV produced extensive damage with a stripe of graphite layer removed [45]. Feddes *et al* managed to change the top graphite layer shift near the twist boundary [49]. They applied a voltage pulse of a few volts to the superlattice region around a screw dislocation site, which initiated the relaxation of the top layer, increasing the superlattice periodicity and eliminating the screw dislocation. By applying a 5 V, 200 ns short voltage pulse, Wei *et al* [66] induced the transition of the occurrence of a superlattice on the HOPG graphite surface from one place to a neighbouring locality.

The disruption brought about by the tip can be ascribed to the tip–sample interaction. Snyder *et al* [67] demonstrated that a small variation in the tip-to-substrate voltage bias (0.1 V–0.24 V–0.1 V, tunnelling current constant at 2.4 nA) gives rise to a reversible transition between the dislocation network (star-shaped network–triangular-shaped network–star-shaped network) (see figure 4 in [67]). This reversible transition was reported to be reproducible during continuous imaging over a period of 2 days without degradation of the network structures. It is believed that the mechanism for the transition between network geometries involves the concerted motion of dislocations within the network, for which the shear stresses resulting from interactions between the tip and graphite surface are held responsible. Snyder *et al* proposed an explanation that when the bias voltage is low (0.1 V), the tip is close to the surface and thus the tip–sample interaction generates shear forces which distort the dislocation network and initiate the transition. This transition is reversed as the bias voltage is raised (0.24 V) because the tip is lifted up and thus the shear forces are cancelled; the restoring forces

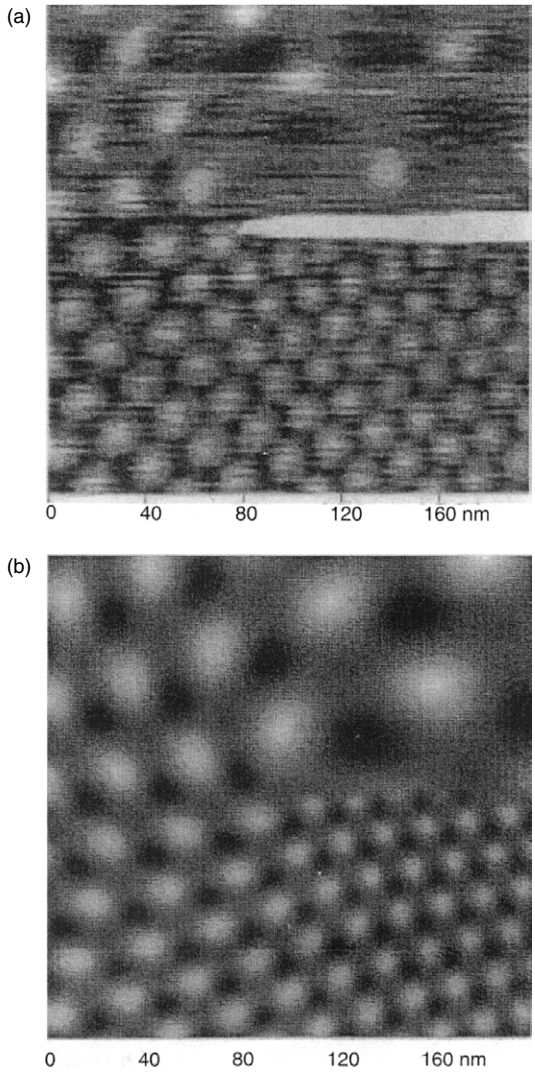

Figure 10. (*a*) The STM image (200 nm × 200 nm) of Feddes *et al* [49] showing a graphite superlattice around a screw dislocation. (*b*) The result of the simulation of the superlattice around a screw dislocation performed by Feddes *et al*. The superlattice constant changes from 18 to 72 nm as it circles around the dislocation. Images reprinted from [49] with permission from E Seiberling.

that result from a local distortion of the network compel the dislocation network back to its previous shape. The shear forces resulting from the STM tip on the graphite surface are estimated to be around 200 MPa, comparable to the 500 MPa value estimated by Gilman [68] for dislocation motion to be achieved at room temperature, larger than the 0.6 MPa value that Soule and Nezbeda [69] found for the macroscopic average critically resolved shear stress for the basal plane of annealed HOPG graphite. Ouseph [46] observed a tip-induced slow correction of rotational misalignment, and a transformation of the superlattice into triangular dislocations, with the tunnelling conditions of a tip bias voltage of 150 mV and a 1 nA tunnelling current. The tip–surface interaction slowly and continuously reduced the misorientation angle of the Moiré pattern over several scans, the superlattice periodicity and the triangle size increased with each scan, and finally the misorientation was corrected uniformly over the whole area of the superlattice. In addition, Ouseph [47], by repeated scanning with a tip bias voltage of 0.15 V, induced the area with normal graphite structure between closely spaced dislocation ribbons to change into a superlattice with the same superlattice periodicity as those of the original ribbons. Such a transformation was ascribed to the tip–sample interaction as well.

On the basis of these findings, it is not surprising that by varying the bias voltage and thus the tip–sample distance, the STM tip can induce shear forces sufficient to move or rotate a graphite layer which will affect a Moiré superlattice pattern.

2.7.2. α–β-site asymmetry. It is well known that the graphite atomic lattice exhibits asymmetry under STM due to the interlayer electronic interaction which divides the carbon atoms on the surface into either α sites or β sites, and β sites appear to be brighter (higher local density of states) in STM images. Such an asymmetry can also be observed on the graphite atomic lattice which is superimposed by a superlattice. Rong and Kuiper [23] quantified the α–β-site asymmetry in the superlattice using this equation;

$$A = (z_\beta - z_\alpha)/(z_\beta + z_\alpha), \tag{13}$$

where A is an arbitrary unit for asymmetry quantification, z_β is the corrugation amplitude for a β site and z_α is the corrugation amplitude for an α site. It is found that the α–β-site asymmetry is maintained throughout the whole superlattice, and in the regions which correspond to g-α-sites in the notation of Xhie *et al* [24] (i.e. the grey regions in the image), the asymmetry is ∼0.56, while in the white regions, corresponding to g-β-sites, it is ∼0.17, which indicates the asymmetry is more pronounced in the greyish regions than in the white regions. Such a difference in α–β-site asymmetry can be explained by the theory of Xhie *et al* [24] described earlier in section 2.5. In g-α-sites, an atom is either above a hole site in the second layer or a β site, and thus the asymmetry is large because in the second layer, the electronic density of states of a β site is much larger than a hole site which leads to a larger difference in density of states on the top layer, whereas in g-β-sites, an atom is either above a hole site in the second layer or a α site and thus the asymmetry is smaller because the difference in electronic density of states is smaller.

2.7.3. Superlattice boundary. Although to date not much discussion has been focused on superlattice boundaries in the literature, a superlattice boundary is an intriguing subject on its own due to the fact that the boundary is the region where the transition from normal graphite to a superlattice occurs. Understanding the nature of these boundaries will help us to understand the origin of the superlattices. As superlattices tend to occur near or along lattice dislocations and defects, in particular steps, a superlattice is mostly terminated by a step edge. Described below are two kinds of commonly observed superlattice boundaries:

Array of bead-like structures. In figure 11(*a*), at the intersection between normal graphite (i.e. a superlattice-free region) and a superlattice (which, in this case has a periodicity of 6.5 nm) there is an uneven boundary along which there is an array of bead-like structures whose corrugation is 0.26 nm, larger than the superlattice corrugation of 0.17 nm.

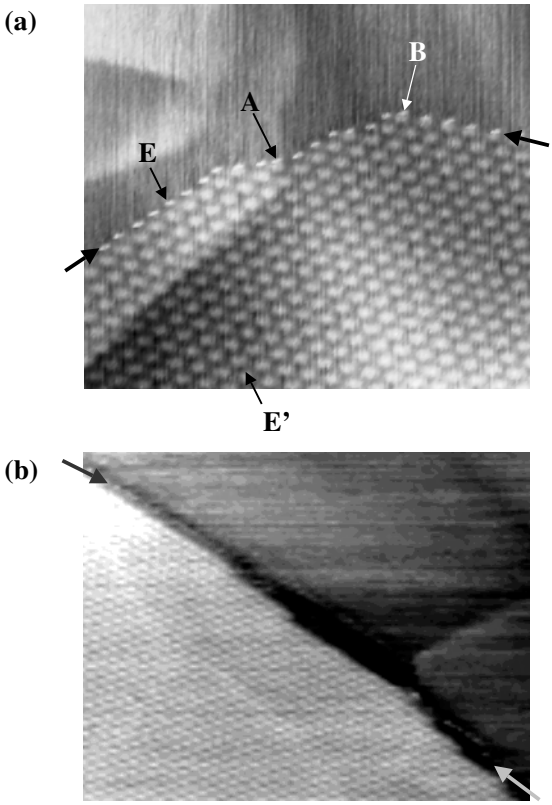

Figure 11. (*a*) 106 nm × 123 nm image, $I_t = 0.5$ nA, $V_t = 230$ mV, periodicity of the superlattice = 6.5 nm. The array of bead-like structures, which is the boundary for the superlattice, is indicated by the thicker arrows. At locations A and B, the bead-like boundary cuts through the bright spots of the superlattice which are of higher energy. If we look at the superlattice row by row along the direction EE′, each bead on the boundary corresponds to each row of the superlattice. (*b*) 200 nm × 254 nm, $I_t = 0.5$ nA, $V_s = 206$ mV, periodicity of the superlattice = 5.3 nm. The zig-zag shaped termination is shown by the arrows.

Observations on this kind of boundary structure have previously been reported in the literature [23, 24, 45, 48, 70]. Going along the boundary indicated by the thick arrows in figure 11(*a*), the position of each bead on the boundary corresponds to each row of the superlattice (along the direction EE′). The boundary intersects localized regions of increased electron density (which appear as bright spots in the image), for instance at locations A and B.

Zig-zag shaped boundary. The superlattice in figure 11(*b*) is terminated by a monatomic step with a zig-zag shape. This kind of zig-zag shaped boundary has been observed previously [20, 53, 71]. In all these results, the zig-zag shaped boundaries appear to go around the superlattice bright spots rather than dissect them.

2.7.4. Dependence of superlattice corrugation amplitude on tunnelling condition. Rong and Kuiper [23] performed an experiment to study the influence of the bias voltage on the superlattice, and they found that as the bias voltage changed from 72 to 535 mV, the superlattice corrugation was reduced by a factor of 3, and the greyish regions (g-α-sites) disappeared (figure 12). The decrease in superlattice corrugation amplitude with increasing bias voltage can be explained by the fact that

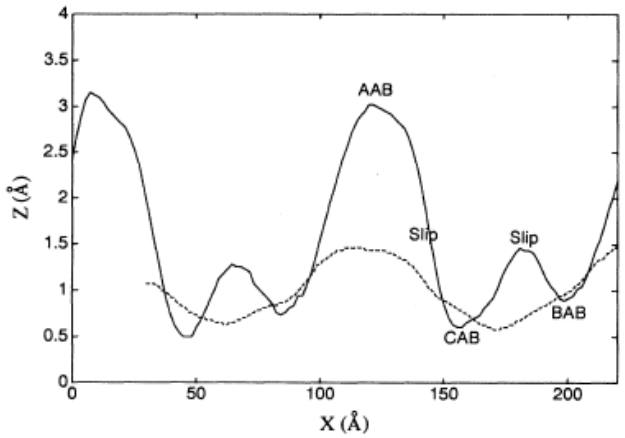

Figure 12. The cross-sections along the maxima and minima of the superlattice. (——) tip bias 72 mV; (- - - -) tip bias 535 mV. Image reprinted from [23] with permission from P Kuiper.

the local density of states on the top layer is only affected by the stacking faults of the underneath layers at the immediate vicinity of the Fermi level, and these densities should be more or less the same when it is far from the Fermi level because they are all mostly dominated by the two-dimensional in-plane interactions [62].

Tunnelling with the same bias voltage but a different tunnelling current may provide completely different images of superlattices. Osing and Shvets imaged a superlattice with a bias voltage of 100 mV and tunnelling current of 2 nA [22]. However, after the tunnelling current was set to 0.1 nA, only the surface topography without the superlattice was observed (compare figures 2(*a*) and (*b*) in [22]). Osing and Shvets concluded that there is a close correlation between the appearance of the superlattice structures in STM images and the tip–sample distance, and the fact that the superperiodic features are observed with a high current indicates that for graphite, the variation of the electron density of states associated with the nanoscale features decays much faster in the direction from the surface to the vacuum than the variation of the electron density associated with the atomic lattice. Such a conclusion is different from the proposal of Kobayashi [61] that a superlattice should not be as obvious when the tip–sample distance is short.

The experimental results of Rong and Kuiper [23] together with those of Osing and Shvets [22] suggests that the superlattice phenomenon decays with a higher bias voltage and lower tunnelling current; both will lead to a larger tip–sample distance, thus attenuating the superlattice corrugations electronically. However, we cannot interpret superlattice corrugations purely from the electrical point of view. The tip–sample mechanical interaction, which is also tip–sample distance dependent (and thus tunnelling condition dependent), is believed to play a significant role, as will be discussed in section 2.9.2. We need to consider both electronic and mechanical effects in order to interpret the superlattice corrugation properly.

The interrelation among superlattices, bias voltage, tunnelling current, and tip–sample distance is an important subject to look at (see section 3.2.1).

Table 2. The reported experimental values of attenuation factors (AF).

Source of data	Tunnelling conditions	Number of overlayers	Attenuation factor
[37]	$V_{tip} = 20$ mV, $I_t = 0.8$ nA	1	2.6
[37]	$V_{tip} = 180$ mV, $I_t = 0.9$ nA	1	2.3
[37]	$V_{tip} = 15$ mV, $I_t = 0.8$ nA	1	2.6
[37]	$V_{tip} = 180$ mV, $I_t = 0.9$ nA	1	1.6[a]
[72]	(not provided)	1	2[b]
[72]	(not provided)	2	4[b]
[43]	$V_s = 206$ mV, $I_t = 0.5$ nA	1	2.3
[21]	$V_{tip} = 178$ mV, $I_t = 2.4$ nA	2	5
[48]	$V_s = 100$ mV, $I_t = 1.0$ nA	1	2.4
[47]	$V_{tip} = 150$ mV	1	1.59
[70]	$V_s = 1200$ mV	1	2.15

[a] This is the AF for the bead-like boundary of the superlattice covered by one overlayer.
[b] The authors of [72] observed the superlattices covered by one and two graphite sheets, and from these data, they proposed equation (15), however, without mentioning explicitly the AFs that they observed experimentally for one and two overlayers. The values in this table are calculated using equation (15).

2.7.5. Attenuation of superlattice corrugation by overlayers. It was observed that when a superlattice is covered by an overlayer, its corrugation is attenuated [21, 37, 48] by a factor, named the attenuation factor (AF), which is the ratio between the corrugations of a direct Moiré pattern and a Moiré pattern covered by an overlayer. The AFs reported in the literature are listed in table 2, where we can see the AF for one layer is about 2.6 while for two layers it is around 5. Equations relating the AF to the number of overlayers are proposed in [43, 72]. Equation (14) was proposed in [43] to predict the attenuation factor (AF_n) from a number of overlayers (n) where K, the attenuation coefficient, was found to be 0.81 by fitting the data of [21, 43] into equation (14) (see table 2).

$$AF_n = e^{Kn} = e^{0.81n}. \tag{14}$$

Figure 13 (solid line) shows a plot of the AF against the number of overlayers (n) according to equation (14), and it predicts the AF for three overlayers to be 11.4. Dalidchik *et al* [72] also suggested an equation to describe the superlattice corrugation covered by n layers:

$$H_n = H_0 \times \alpha^n, \tag{15}$$

where α is found to be around 0.5 from their own experimental data. If we interpret equation (15) in terms of the AF, i.e. $AF = H_0/H_n$,

$$AF_n = 2^n. \tag{16}$$

Figure 13 (dashed line) shows a plot of the AF against the number of overlayers (n) according to equation (16), and it calculates $AF_1 = 2$, $AF_2 = 4$. The AF for three overlayers is predicted to be 8, smaller than the one from equation (14). Both equations (14) and (16) exhibit an exponential relationship between the AF and the number of overlayers, which is not surprising as the electronic influence from a subsurface layer is expected to decay exponentially with its depth. Considering the AF for four overlayers to be approximately 20.8 (the average from equations (14) and (16)), a superlattice covered by four overlayers would be very difficult to observe as its corrugation amplitude is likely to be less than 0.5 Å, which is even smaller than graphite atomic lattice corrugation.

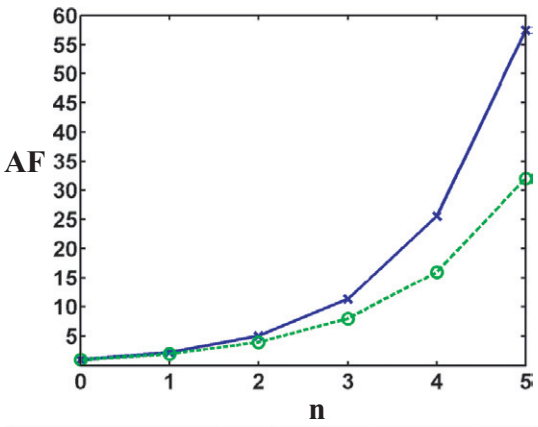

Number of layers (n)		0	1	2	3	4	5
Attenuation factor (AF)	Eq. (14) $AF_n = e^{0.81n}$	1	2.25	5.05	11.4	25.5	57.4
	Eq. (16) $AF_n = 2^n$	1	2	4	8	16	32

Figure 13. Plot of AF against the number of overlayers (n) using equations (14) (——) and (16) (- - - -). The values of each data point are shown in the table below the graph.

Although the corrugation of a direct Moiré rotation-induced superlattice (without overlayer) is voltage dependent, the voltage dependence of a covered Moiré-induced superlattice is rather weak [37]. As a consequence, the AF depends on the bias voltage, which is reflected by table 2, wherein we can see, even for the same number of overlayers, the AF changes slightly according to the tunnelling conditions.

2.7.6. Preparation of a superlattice. A graphite superlattice is caused by dislocations which occur during the growth of the crystal or from the cleavage process, upon which we have little control. Therefore, a graphite superlattice is perceived to be a natural structure which cannot be prepared in a controlled manner. However, efforts have been made to artificially produce graphite superlattices.

Beyer *et al* [17] cleaved a graphite surface with a shear force, tearing apart a graphite monolayer which folded back onto the graphite substrate with a small rotation. A superlattice

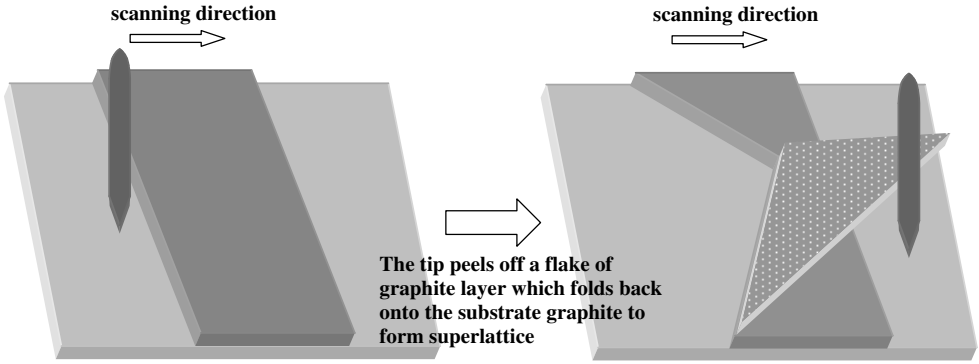

Figure 14. Explanation of Gan's method by using the STM tip to fold over a graphite monolayer to form a superlattice.

was formed on the rotated layer and ended sharply at the borders of this layer. Beyer *et al* [17] suggested a few advantages of the method of producing a superlattice on graphite by cleaving the surface with a shear force: (1) The part of the layer which is folded back and rotated will have a hole associated with it, that is an indication that the folded layer was originally part of the topmost layer. (2) The misorientation angle between the graphite substrate and the folded part can be determined from the STM image. (3) From the surface topography shown in the STM image, we can know that there is a relative rotation of two adjacent layers. (4) A comparison is available to check whether the superlattice is confined within the folded layer or it also occurs in other areas.

Gan *et al* [18] created a superlattice structure by scanning several times against a step of graphite in the constant current mode and tearing off a part of the graphite layer which folded back onto the graphite substrate and formed the superlattice. The experiment is illustrated in figure 14. This provides a means of preparing a superlattice on graphite. However, there is not much control on the exact position and the periodicity of the superlattice to be generated as we cannot precisely manipulate the location and the angle of the tearing of a graphite layer.

As in the experiment of Gan *et al*, Bernhardt *et al* [52] managed to manipulate nanometre sized graphite sheets consisting of only one or a few graphite monlayers with the STM tip to create a superlattice with varying periodicity. This provides a promising means of artificially producing graphite superlattices. In the first step, they located the tip over some stepped and structured regions on the graphite surface and looked for appropriate graphite flakes, while the tunnelling voltage was held at about 800–1000 mV (tunnelling current 1 nA) so as to minimize tip–sample interaction. The tip–sample interaction on graphite increases dramatically as the tunnelling voltage is set below 500 mV (tunnelling current 1 nA) [73–75]. Therefore in the second step they made use of this effect and scanned over weakly bound graphite sheets with decreased tunnelling voltage (370 mV, 1 nA), i.e. small tip–sample distance, and managed to fold back the graphite sheets with a height from one to three monolayers. During the whole procedure the feedback system was not interrupted, and the folding direction can be controlled to a certain extent by variation of the scanning direction.

Exposing graphite to chloroform was demonstrated to produce a high concentration of superlattices [70], which can be another means of artificially producing graphite superlattice structures. The graphite samples were cleaved by adhesive tape. The clean surfaces were then exposed to chloroform through drop-wise deposition or submersion. The samples left to soak in chloroform for several weeks showed a very high concentration of various kinds of defects, including hexagonal superlattices, glide defects and many types of hole. Even in samples exposed to only modest amounts of chloroform (through drop-wise deposition), graphite superlattice structures could still be observed after cleaving off several layers of graphene. The effect of the chloroform is believed to extend well into the crystal bulk, generating several kinds of defect including Moiré superlattices.

2.7.7. Odd–even transition. The theory of Moiré rotation pattern originally did not illustrate the whole picture of a superlattice superimposed on the atomic lattice because it could not explain the fact that in some instances (figure 2(*a*) in [23], figure 3 in [24], figure 11 in [76]), a wavy behaviour of the atomic rows was seen with the presence of the superlattice. In light of that inadequacy, Osing and Shvets completed the story by proposing the odd–even transition phenomenon to explain the wavy appearance of the atomic rows [22]. The idea of the odd–even transition theory is elucidated by the model in figure 15, from [22]. In the model there are two graphite layers rotated with respect to each other, rearranging the stacking sequence, which in turn modifies locally the density of states. Such modification brings about two different groups of atomic lattice with different stacking and thus different density of states. In region 1, the layers are of AA stacking (an atom of a layer is on top of the atom of another), whereas in region 2, the layers are of normal AB stacking. The atomic corrugation in region 1 is smaller because all atoms are in α sites and thus have a similar density of states. On the other hand, in region 2, the atomic corrugation is more obvious as α–β-asymmetry applies here, which gives rise to the usual atomic graphite lattice (highlighted as a centred hexagon in figure 15). Saadaoui *et al* [77] have shown that the β sites in a region of type 2 become the α sites in the neighbouring region 2. Nysten *et al* [76] clarified this point that, if the hexagon atoms are denoted from 1 to 6, those being the β sites will be, for example, the 1–3–5 atoms in one area and will be the 2–4–6 atoms in the neighbouring one. By observing the schematic model, we can see there is a shift between the atomic rows of two adjacent regions of type 2 (indicated by the thick solid line

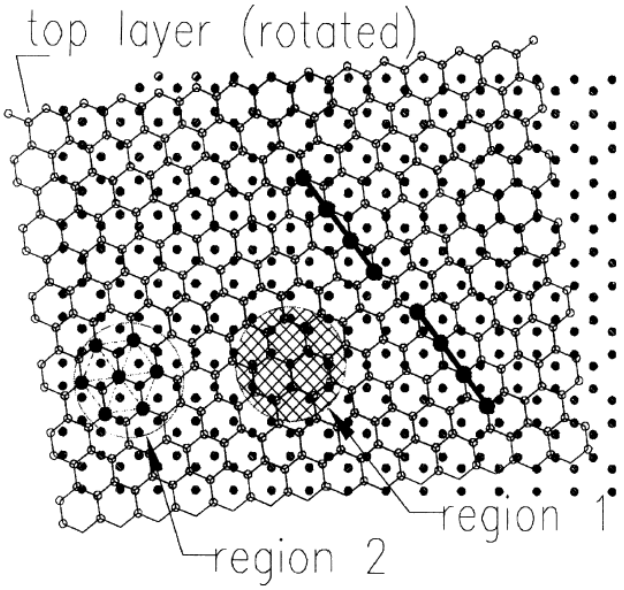

Figure 15. Schematic illustration of the odd–even transition phenomenon. The two graphite layers with a rotation angle between them produce a Moiré superlattice pattern. There are two types of regions: region 1 with the AA stacking sequence which leads to an α site character for every atom; region 2 with the usual AB stacking which gives rise to normal α–β-asymmetry, producing the usual graphite atomic lattice in STM images. There is a shift between the atomic rows of two adjacent regions of type 2 indicated by the thick solid line. Image kindly supplied by I V Shvets [22].

in the schematic). This shifting of atomic rows is the origin of the wavy appearance in some STM images of the atomic lattice on the superlattice, yielding the odd–even transition phenomenon. Osing and Shvets concluded that for a Moiré superlattice pattern superimposed onto the atomic graphite lattice, there must be at least two layers in the AB-stacking sequence on the surface to constitute the normal hexagonal lattice without a wavy appearance in an STM image. This phenomenon is proven by the simulation model as discussed in section 2.6.3.

2.7.8. Adsorption sites for particles. As a superlattice periodicity is comparable to particles, it is interesting to see the influence of the superlattice structure on the deposition of the particles on the surface. Xhie *et al* deposited some cobalt particles with sizes of 1–5 nm onto a graphite superlattice with periodicity of around 3.8 nm, and the cobalt particles settled on top of the peaks of the superlattice [24]. Previous experiments showed that single atoms and atomic dimers of noble metals prefer β sites of the graphite atomic lattice because of the higher local density of states at the Fermi level compared with the other sites [78, 79]. The size of cobalt particles is too large compared to the graphite atomic lattice to adsorb to any atomic sites. The periodicity and symmetry of the superlattice makes it possible for the cobalt particles to position themselves on the g-β-sites whose local density of states at the Fermi level is larger than at the other sites. The dependence of the adsorption sites on graphite for atoms and clusters on the local density of states at the Fermi level is potentially a way of manipulating the deposition of the particles onto the surface which makes a superlattice a useful template for patterning particles on a surface. This will be further discussed in section 3.2.3.

2.8. Controversies about graphite superlattices

Although the Moiré rotation pattern assumption is widely accepted as the primary cause of graphite superlattices, some experimental and simulation works were reported which contradict the Moiré pattern explanation.

2.8.1. Formation of superlattice without rotation of graphite layer. Patrick *et al* observed a superlattice structure in an experiment involving the liquid crystal 4-octyl-4′-cyanobiphenyl (8CB) and monolayer-deep etch pits on graphite using STM [80]. A terrace on the graphite showed a superlattice with a periodicity of 54 ± 1 Å a corrugation amplitude of 1.4 ± 0.5 Å, having a hexagonal symmetry. This superlattice is superimposed onto the underlying atomic graphite lattice, with both the superlattice structure and atomic lattice visible in the STM images. In the middle of the terrace was a 325 Å diameter etch pit where a normal graphite atomic lattice was imaged without any superlattice structure, which inclines us to expect that the graphite layer at the bottom of the pit should have a different orientation from the top terrace layer as only the top terrace layer exhibits the superlattice. However, by comparing the atomic resolution images obtained from the bottom of the pit and the terrace with the superlattice, the atomic lattices in these two layers are aligned to each other without misorientation. Patrick *et al* believed that a simple Moiré rotation pattern assumption cannot explain this contradication and some other mechanism must be involved in the formation of the superlattice in this case.

However, there are two points worth further consideration. First, the depth of the pit is not a monolayer but 4.8 ± 1 Å instead, which is around 43% larger than the interlayer spacing of graphite (3.35 Å). Such a difference was ascribed to the presence of the superlattice. Nevertheless, it is possible that during the etching or the deposition of the liquid crystal molecules, some species went underneath the bottom of the pit and thus lifted the layer by about 1.5 Å. Moreover, the heating process whereby the graphite was heated in air to above 550 °C might have disrupted the normal graphite layered structure at the top few layers. Since this particular piece of graphite was prepared in a more complicated way rather than by simple cleaving and similar experimental results on graphite superlattices have not been reported elsewhere, we may regard this non-Moiré pattern-induced superlattice as an exception where the etching and deposition of a liquid crystal produced such a peculiar superlattice.

2.8.2. Corrugation conservation phenomenon. It is reported in the literature that when a superlattice traverses across a graphite step, its corrugation will be attenuated by the overlayer by a factor of around 2. However, in [43], a superlattice which stretches across a step was observed without any detectable attenuation in its corrugation amplitude (figures 16(*a*) and (*b*)). According to equation (14), proposed in [43], the ratio of the amplitudes of the corrugation on the two sides of the step should be $\exp(K)$. To fit the data in this case then, the attenuation coefficient, K, will have to be extremely small, of

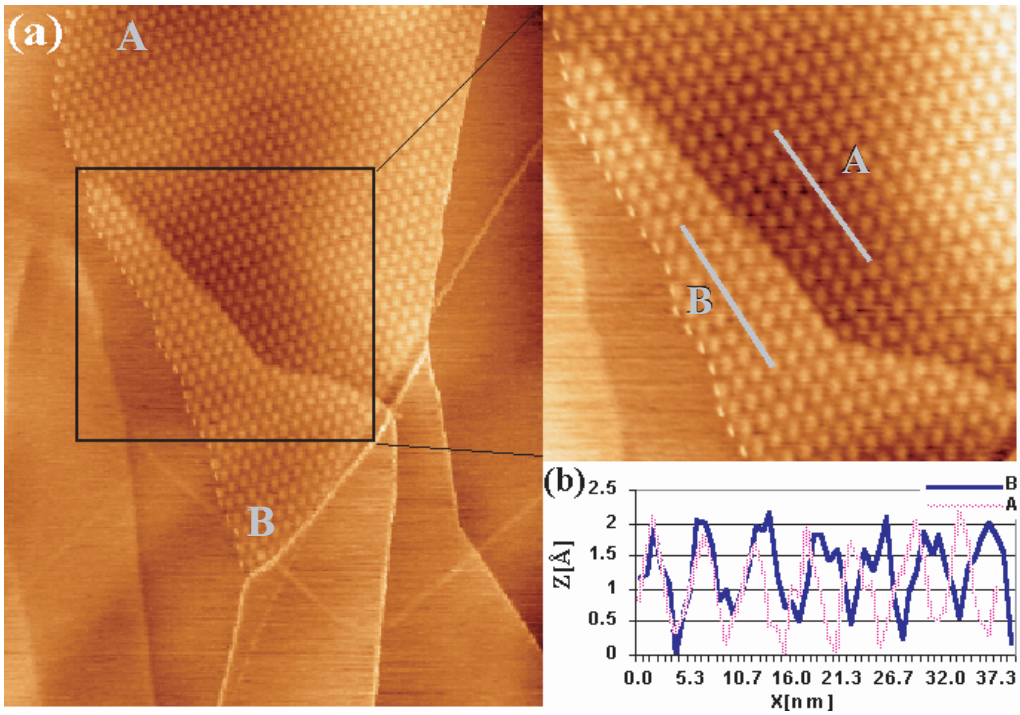

Figure 16. (*a*) 319 nm × 300 nm image ($I_t = 0.5$ nA, $V_t = 230$ mV) of graphite with the superlattice structure covering an about 200 nm^2 area. The zoom-in on the right shows the superlattice in regions A and B more clearly. The superlattice extends across the monoatomic step edge without much attenuation as we can observe in the cross-section in (*b*). (*b*) shows the cross-sections in regions A and B.

the order of 0.03 or less. This is obviously significantly smaller than the value of 0.81 for normal cases. This corrugation conservation phenomenon is rather complicated to understand, and the authors can only speculate that in this particular case, the superlattice is not entirely due to a Moiré rotation.

2.8.3. Correlation between local stacking and density of states. Rong and Kuiper [23] categorized local stackings of graphite superlattices in a way different from that of Xhie *et al* [24]. Xhie *et al* categorized all the surface-atom sites into M-α, M-β and M-h sites, on the basis of the surface-atom location relative to the AB-stacked substrate graphite crystal (figure 7(*d*)), whereas Rong and Kuiper did the categorization of surface atoms according to the local stacking of the topmost three graphite layers and formed four groups: AAB, slip-AB, AB (normal stacking) and CAB stacking (figure 17). There are four groups of surface-atom sites for the model of Rong and Kuiper, but there are only three for that of Xhie *et al* because Rong and Kuiper distinguished two types of valleys with different intensities in STM superlattice images while Xhie *et al* regarded all the valleys as of the same type.

The band-structure calculation using a tight-binding description of the electronic structure [62] indicates that AA-stacked graphite has a density of states at the Fermi level of 0.0085 states eV^{-1}, which is three times larger than that of AB- or CAB-stacked graphite, in contrast to the expectation from an analogy to α sites (the analogy that Xhie *et al* used in their model). The density of states at the Fermi level for normal AB-stacked graphite is 0.0033 states eV^{-1} (0.0056 states eV^{-1} for β sites and 0.0011 for α sites, which averages to 0.0033 states eV^{-1}), and it is 0.0021 states eV^{-1}

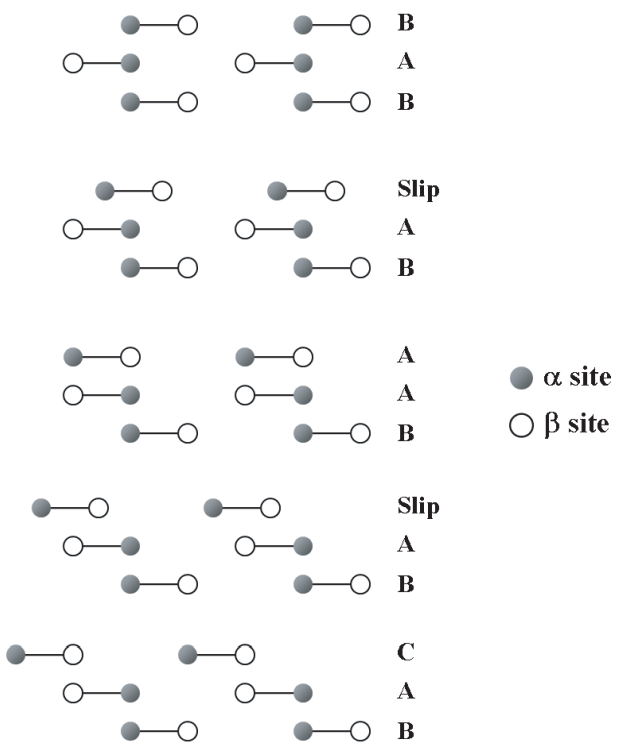

Figure 17. Different stacking structures of graphite are produced by sliding the top graphite layer by different distances. Grey circles and white circles are α and β sites of AB normal stacking, respectively. Based on this model, Rong and Kuiper [23] categorized the atomic sites in a superlattice into BAB, slip-AB, AAB and CAB and assigned them with different intensities in STM images according to the band-structure calculation of Charlier *et al* [62].

for CAB-stacked graphite. As such, Rong and Kuiper assigned the brightest peaks of a superlattice in STM images to AAB stacking, the second deepest valleys to normal AB stacking, and the deepest valleys to CAB stacking (figure 12). The remaining slip-AB stacking is assigned to be the second brightest peaks of a superlattice.

If we translate Xhie *et al*'s model into Rong and Kuiper's model, M-β-sites (brightest superlattice spots in the Xhie *et al* model) correspond to AB normal stacking which are the second deepest valleys in Rong and Kuiper's model, M-α-sites (medium brightest superlattice spots) correspond to CAB stacking which are the darkest valleys, and similarly, M-h-sites (darkest holes) are AAB stacking which are the superlattice peaks in the other model. Rong and Kuiper's model appears to be more convincing as it is supported by a first-principles calculation while Xhie *et al*'s model is only based on the deduction that the interlayer electronic interaction for the top rotated layer from the substrate should be the same as the interaction for normal AB-stacked graphite: atoms above hole sites are the brightest in the STM images, atoms above α sites are the second brightest, and atoms above β sites are the darkest. Whilst Rong and Kuiper referred to the work of Charlier *et al* [62] as the basis of their model, the calculation in [62] was based on the models in which the AAA, AB or CAB stacking is maintained throughout the whole graphite crystal rather than just the top three layers with the bulk in normal AB-stacking. In other words, for a real superlattice, its stackings are ABABAB..., CABABAB... and AABABAB..., but the calculation by Charlier *et al* is for ABABAB..., CABCAB... and AAAAAA.... Although they look similar for the first three layers, the structures of the bulks of the crystal models are completely different. Such a difference may render Rong and Kuiper's model questionable, and definitely further rigorous theoretical calculation is needed for justification.

2.8.4. Unusual aspects of superlattice structures on HOPG reported by Cee et al. Cee *et al* reported a few unusual aspects of superlattice structures which cannot be explained by the generally accepted Moiré rotation pattern hypothesis [63]. They used the simulation model to generate a superlattice with the contribution of each graphite layer decreasing in weight with its depth from the surface ($W_2 = 0.5$ and $W_3 = 0.125$, normal weighting). The resulting simulated pattern is a superstructure of hexagonal symmetry, unlike the three-fold symmetry on the experimentally observed superlattices where three of the six maxima are more intense in STM images. Then they carried out another simulation with an exaggerated difference in the relative contributions of the second and third layers ($W_2 = 0.125$ and $W_3 = 0.25$, exaggerated weighting), which does not agree with the idea that the electronic influence from a lower layer should be less as the interlayer electronic interaction decays with distance. Surprisingly, this superlattice simulated with counterintuitive weightings appears to exhibit three-fold symmetry as observed using STM. Consequently, this simulation result brings out the contradiction that the Moiré rotation pattern assumption cannot be true unless the electronic contribution from the third layer is larger than the second layer, which is obviously non-physical.

In the STM images on etched graphite, Cee *et al* observed two superlattices in contact on the same layer, each with a different periodicity, separated by a well-defined boundary (figure 5 in [63]). Without apparent topographic defects in the area, for instance, buckling, cracking or a grain boundary of the graphite layer, a change in the rotation angle of the graphite layer is unlikely. The observation is thus beyond the explanation of Moiré rotation assumption. On another surface of graphite deposited with a liquid crystal molecule 4′-octyl-4-carbonitrile (8CB), Cee *et al* also imaged a transient superlattice in the middle of a thin strip of graphite with two defects confining the superlattice and causing stretching at the edges (figure 6 in [63]). They then applied a voltage pulse from -0.4 to -4 V several times at the middle of the superlattice. This action made the defect marking the left boundary of the superlattice and the superlattice itself vanish. However, the vanishing did not come with the change in the orientation of the terrace strip where the superlattice was, which is not compatible with the expectation of the Moiré pattern hypothesis that the vanishing of the superlattice should have come with the change of the orientation of the terrace strip. In addition, on a graphite sample which was etched by heating to 650 °C in air, where much of the topmost layer was etched away with several isolated islands of graphite layer remaining, a superlattice existed on one of the islands, while another island nearby on the same graphite layer did not contain any superlattice (figure 7 in [63]). Cee *et al* stated that Moiré rotation could not be the cause of the superlattice because the whole layer, and thus both islands, would otherwise be expected to contain a superlattice, and secondly the possibility of a grain boundary was excluded because of the mode of etching of the uppermost layer.

The experimental and simulation results presented by Cee *et al* were arguments against the Moiré rotation pattern assumption, which suggests we should rethink the origin of graphite superlattices. Nevertheless there are different accounts of their results.

Recently, a simulation result different to that of Cee *et al* was reported [54]. Using the same model based on equation (3), the same simulation with the same exaggerated weightings and rotation angle was performed; however, a different result was obtained. In [54], the difference in contrast in the simulated superlattice between using the normal weightings ($W_2 = 0.5$ and $W_3 = 0.125$) (figure 18(*c*)) and the exaggerated weightings ($W_2 = 0.125$ and $W_3 = 0.25$) (figure 18(*d*)) is not very significant. Cee *et al* did not specify in their paper how they simulated the relative shift between alternating graphite layers, which may be the reason for the difference. It is also found that the atomic lattice of the superlattice simulated with the exaggerated weightings (figure 18(*b*)) does not have as obvious a three-fold symmetry as that simulated with the normal weightings (figure 18(*a*)), and indeed, it is difficult to observe the three-fold symmetry in figure 18(*b*). This is because the three-fold symmetry of the atomic lattice arises from the α–β asymmetry which in turn is due to the subtraction of the electronic density of states of the second graphite layer from the first; by using the exaggerated weightings of $W_2 = 0.125$ (instead of 0.5 for normal weightings), the effect of the subtraction is significantly diminished. Therefore the simulated superlattice using the exaggerated weightings is counterintuitive. The simulation results [54] show that the normal weightings which

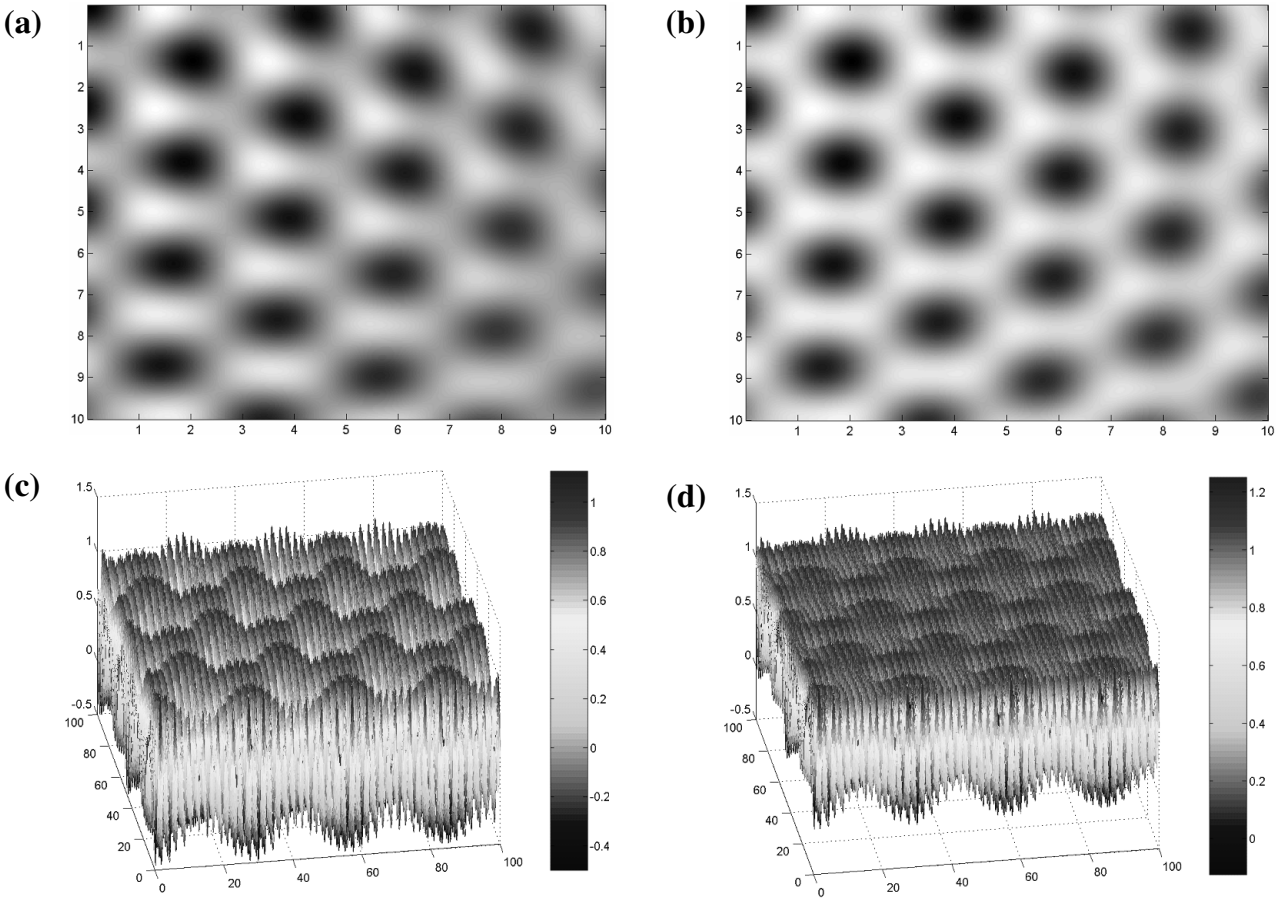

Figure 18. Comparisons between the normal weightings and exaggerated weightings. (*a*) 1 nm^2 superlattice area simulated with the normal weightings. (*b*) 1 nm^2 superlattice area simulated with the exaggerated weightings. (*c*) 10 nm^2 superlattice area simulated with the normal weightings. (*d*) 10 nm^2 superlattice area simulated with the exaggerated weightings. All rotation angles are 5° (periodicity 2.82 nm). The three-fold symmetry of the atomic lattice is more distinct in (*a*) than in (*b*). The contrast in height is higher in (*c*) than in (*d*).

are consistent with the Moiré rotation pattern assumption can produce a more physically realistic graphite atomic lattice and superlattice structures.

2.8.5. Superlattice with square symmetry. Apart from hexagonal superlattices, cubic superlattices were observed on graphite. Oden *et al* [50] obtained the images of the square lattice under triply distilled 18 MΩ water, with $Pt_{0.7}Ir_{0.3}$ tunnelling tips coated with Apiezon wax up to the tip apex and the Faradaic leakage current limited at 10 pA; the bias voltage between the tip and substrate was 0.1 V. Around 1% or less of the graphite surface was covered with square superperiodic features, with observed periodicities ranging from approximately 45 to 440 Å, with corrugation amplitudes distributed from 2 to 5 Å. In terms of periodicity and corrugation amplitude, the square-arranged superlattices are similar to normal superlattices, apart from the fact that these square superlattices do not have hexagonal symmetry and thus cannot be explained by the Moiré rotation pattern assumption.

However, atomic resolution images were not obtained on the square lattices, and thus one cannot rule out the likelihood that the square superlattices are due to adsorbed species from the solution. Another possibility is that the solution molecules go into the graphite interlayer space and cause surface deformation, which gives rise to this kind of square superlattice.

2.9. Unexplained phenomena

There are some phenomena concerning graphite superlattices which, while not contradicting the Moiré rotation pattern assumption, still remain unexplained.

2.9.1. More metallic nature of the superlattice than normal graphite. In their experiment, Kuwabara *et al* performed current–voltage spectroscopy measurements on both the superlattice region and the adjacent normal graphite region, and the measurements indicate that the superlattice region is more metallic than normal graphite, while there is no appreciable difference between the peaks and valleys of the superlattice [20]. Rong and Kuiper [23] demonstrated that the Moiré-induced superlattice pattern changes its shape with variation of the bias voltage, which indicates that different stacking configurations of graphite layers have different I–V characteristics. This can possibly explain the more metallic nature of a superlattice as the stacking configuration of a superlattice is different from that of normal graphite.

2.9.2. Superlattice large corrugation amplitude. The origin of the anomalously large corrugation amplitude in some superlattices is not well understood. While the observed corrugation of the graphite atomic lattice is around a few angstroms (amplified by the tip–surface interaction), the corrugation of a superlattice can be several nanometres. This is not understandable simply by considering surface morphology and density of states; rather, it is believed to be associated with tip-induced mechanical deformation of the surface [20]. According to the Moiré rotation hypothesis, the formation of a superlattice is due to a thin layer of graphite misoriented with respect to the bulk crystal. It is reasonable to expect that, if the corrugation of graphite atomic lattice can be attributed to the STM tip-induced surface deformation, the tip would bring about an even larger surface deformation on a superlattice region. Indeed, superlattice corrugations and atomic corrugations of graphite exhibit a similar dependence on the bias voltage; both corrugations decrease in amplitude as the bias voltage is increased [19, 23, 46], which can be supportive of the argument that the large superlattice corrugation has the same origin as the giant corrugation of the atomic lattice which has been routinely observed on a graphite surface using STM. Garbarz *et al* [19] showed that there exist interatomic forces between the tip and surface and such forces vary rapidly as the tip-to-surface distance varies. As such the vertical displacement of the tip will be amplified and induce a large elastic deformation. The deformation is particularly pronounced at dislocation sites since the softness of the crystal is increased locally by the mobility of a dislocation. Beyer *et al* attributed the giant corrugation of the superlattice to the effect of the elastic tip–sample interaction as well [17]. The tip–sample interaction is dependent on the tip–sample distance; when the distance is smaller (larger), the interaction is stronger (weaker) and thus the superlattice corrugation becomes larger (smaller). As discussed in section 2.7.4, electronic effects depending on the tunnelling conditions are a factor in the apparent superlattice corrugation; together with the tip–sample interaction, they give a more comprehensive idea about the origin of superlattice corrugations.

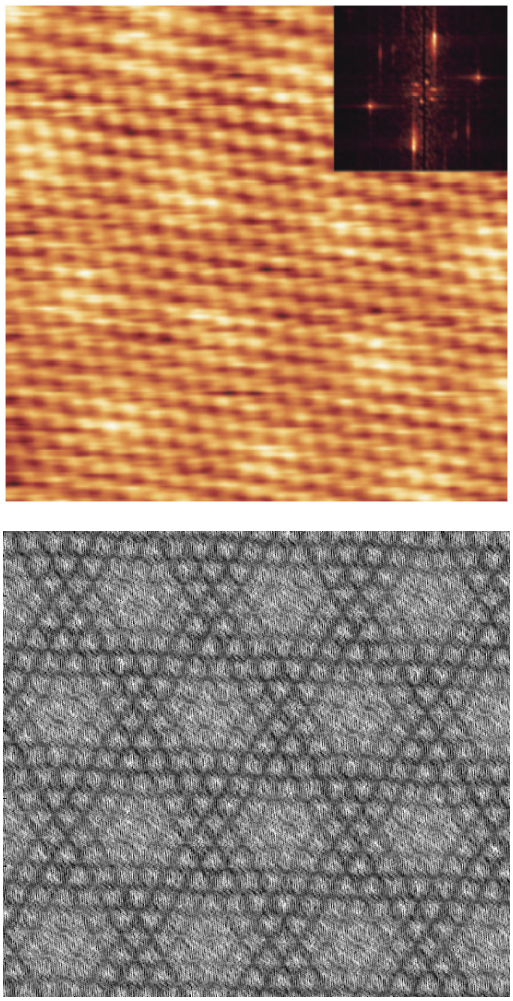

Figure 19. (*a*) 63 nm × 63 nm, $V_s = +700$ mV. Coexisting superlattices with periodicities of 19.2 and 3.25 nm observed by Ball *et al*. The inset shows the corresponding FFT spectrum. Image reprinted from [70] with permission from S J Ball. (*b*) A superlattice with an area of 67 nm × 67 nm simulated with the top layer rotated 4.3° and the second layer rotated 0.73° with respect to the third layer, respectively.

2.9.3. Coexisting superlattices. In most of the cases reported, only one superlattice exists in an area at a time. However, it has been reported that two superlattices with different periodicities coexist on the same area of graphite. Xhie *et al* observed that on top of a superlattice (giant lattice) with a periodicity of 3.8 nm, there is another superlattice (supergiant lattice) with a slightly distorted hexagonal pattern with a periodicity of approximately 15 nm (figure 6 in [24]). The corrugation of the supergiant lattice is around 0.1 nm, which is 1/10 of the corrugation of the giant lattice. Xhie *et al* attributed this phenomenon to the strain produced by the small rotation of the top layer [24]. It is also possible that the top two graphite layers are rotated with different angles with respect to the third layer, resulting in two overlapping Moiré patterns, while the slight distortion of the hexagonal pattern of the supergiant lattice maybe caused by the strain due to the misorientation of the graphite layers. Ball *et al* [70] observed a similar phenomenon comprising two overlaid hexagonal superlattices of different periodicities of 3.25 nm (corrugation 0.1 nm) and 19.2 nm (corrugation 0.2 nm) (figure 19(*a*)). They also attributed it to the two rotated graphene planes with different rotation angles.

Such an effect can be studied with the model which we have described in section 2.6. A superlattice can be simulated with the top two layers rotated with different angles with respect to the third layer. In this way, we will be able to see whether two superlattices can coexist in the same area by Moiré rotation. We have carried out a simulation to model the coexisting superlattices (figure 19(*a*)) observed by Ball *et al*. The simulated area is 67 nm × 67 nm, similar to the 63 nm × 63 nm image of the coexisting superlattices (figure 19(*a*)). The first graphite layer is simulated with a rotation angle of 4.3°, while the second graphite layer is simulated with 0.73°, both with respect to the third layer. Normal weightings of $W_2 = 0.5$ and $W_1 = 0.125$ are used, and the simulation result is shown in figure 19(*b*). The simulated results show coexisting superlattices with periodicities and hexagonal symmetries similar to those observed by Ball *et al*.

3. Outlook and conclusion

3.1. Significance of findings on graphite superlattices

An understanding of the superlattice phenomena on graphite is of paramount importance for a better understanding of the STM imaging process at the atomic scale. STM is generally believed to be sensitive to the local density of states near the Fermi level on the topmost layer of a surface. However, the observation of Moiré rotation-induced superlattices indicates that the interlayer electronic interaction with the subsurface layers can lead to periodic modulation of the density of states on the topmost layer. This carries a profound implication for STM images because STM images do not just reflect the topmost surface condition but those of the subsurface layers as well. In addition, the apparent corrugation in STM images is often not the original true corrugation of the sample surface but is due to the tip–sample surface deformation effect. Since the early days of STM, graphite has been a surface of extensive study. Graphite is also commonly used as a substrate for the study of various kinds of adsorbates including organic molecules and biological species. However, in certain cases, it can be difficult to distinguish between specific adsorbate structures (especially periodic) and a superlattice on a graphite surface.

The work on superlattices provides a basis for understanding surface electronic structures with different subsurface layer configurations, which constitutes an important part of the principle of the STM technique. Graphite superlattice systems are useful for a comparative study of the three stacking structures, AAB, CAB and BAB [23]. This may be useful, as we have mentioned earlier in section 1.3, for the manipulation of material properties by reconfiguring the stacking sequence of layered structures of graphite.

3.2. Future direction

3.2.1. Possible experiments to do

Develop experimental protocol for producing superlattices. As discussed in section 2.7.6, there exist methods to artificially produce graphite Moiré superlattices. In addition to cleaving a graphite with shear force, it is possible to fold back a graphite sheet with a slight rotation to artificially produce a superlattice structure on graphite by scanning with a STM tip. A systematic way of routinely constructing a superlattice would be of tremendous help for understanding the mechanism of superlattice structures as it will enable us to establish a superlattice in the desired pattern for experiments. As such, an established experimental procedure, entailing the configuration of the tunnelling conditions, feedback control parameters, scanning speed and appropriate choice of area, for engineering a superlattice on a graphite surface would be a useful research subject to explore. The approach of exposing graphite to chloroform is also a practical route of generating Moiré superlattices. More research effort is needed to identify the mechanism for the introduction of defects by chloroform including superlattices. Also, it would be of interest to investigate if there is any correlation between superlattice properties like corrugation amplitudes and periodicities and the exposure duration to chloroform.

Experimentally verify coexisting superlattices. By using Gan's method, it is possible to tear off one layer first, and then another layer to be placed on top of the first one with a different rotation angle. In this way, the rotation angle between the first and second layer is different from the rotation angle between the second layer and the substrate. According to the Moiré rotation pattern assumption, we should be able to see two coexisting superlattices resulting from the coupling of the first layer with the substrate and the second layer with the substrate, respectively. It would be interesting to verify it experimentally as this will show the origin of coexisting superlattices in the same area and the influence of the electronic effect from the third layer to the topmost layer under STM. A simulation model with the second and third layers rotated with respective angles to check if the coexisting Moiré patterns are theoretically possible will be supplementary to the experimental work.

Interrelation among superlattices, bias voltage, tunnelling current and tip–sample distance. From the results of Rong and Kuiper and Osing and Shvets (see section 2.7.4), we know that the configuration of the bias voltage and tunnelling current has a role to play in STM images of superlattices. This relationship depends upon the variation of the electron density of states of a superlattice with the bias voltage and tunnelling current. Research work on this topic will enable us to understand the influence of the tunnelling conditions on the interlayer electronic interaction of graphite which gives rise to the variation of the resulting Moiré superlattice pattern. However, no systematic study has been conducted so far.

To investigate this subject, when a superlattice is being imaged using an STM, the tunnelling condition can be varied with the tunnelling current from 0.01 to 3 nA, the bias voltage from −2 to +2 V, and the corresponding superlattice periodicity, orientation, corrugation amplitude and atomic corrugation recorded. In this way we can see how the superlattice changes with the tunnelling condition and compare the rates of decay of the electron density of states associated with the superlattice and the atomic lattice in the direction from the surface to the vacuum. We can then analyse the correlations between superlattices and these different parameters.

3.2.2. Possible theoretical calculations to do.

Continuation of the theoretical work of Kobayashi. As discussed earlier, Kobayashi [61] pointed out that nanoscale waves propagating through many layers without decay can be the cause of superlattices. His theory provides an alternative route to explaining superlattices observed in STM; nevertheless, further theoretical work is needed to delineate the theoretical correlation between the superlattice structures observed in STM images and the nanoscale structures buried deep in the bulk, for instance what kind of nanoscale structures does it have to be in order to form Moiré superlattices on the surface, do the nanoscale structures have to be an array of structures, and what is the relationship between the periodicity and corrugation of a superlattice and nanoscale structures. Should the correlation be elucidated, the aspects of the relationship between superlattice corrugations and number of overlayers and the dependence of the Moiré pattern on the

tip–sample distance are worth further investigation because, in this respect, experimental results conflicting with Kobayashi's theory have been shown as mentioned in section 2.7.4.

Superlattice corrugation. The large superlattice corrugation is speculated to be related to tip–surface mechanical deformation like the mechanism for giant atomic corrugation for graphite. However, there is no theoretical work to support such speculation. In this regard, a simulation should be performed which considers a rotated top graphite layer misoriented with respect to the bulk, with the commonly used tunnelling conditions used to observe superlattices (table 1), and in the framework of the Moiré rotation pattern assumption to study the tip–surface interaction and its effect on the resulting superlattice corrugation.

Influence of tip shape and tip–sample distance. The simulation model combined with integration of the tip shape and tip–sample distance enables us to investigate their influence on the resulting STM images of superlattice structures. Rong [37] reported two kinds of patterns for superlattice bright spots: triangular and circular shapes. Distorted hexagonal arrangements of superlattices were sometimes observed [24, 45]. Both these phenomena may be attributable to the shape of the STM tip. The knowledge of the influence of tip shape on superlattices will help us to interpret the STM images properly with more insight. Since there is experimentally no way of preparing a tip with a specific shape, theoretical calculations using the simulation model described in section 2.6 offer a possible route for the relevant investigation. Moreover, this model enables us to simulate the relationship between the tip–sample distance and the resulting STM images which would be complementary to the above-mentioned theoretical study on the correlation between the tip–surface interaction and the superlattice corrugation with various tunnelling conditions (section 3.2.2); together they will present the whole picture of the tip-imaging mechanism of superlattices.

Electron density of states with different stacking faults. Xhie *et al* [24] and Rong and Kuiper [23] used different models to explain the correlation of the local stackings with the local density of states, and they arrived at different conclusions as discussed in section 2.8.3: Xhie *et al*'s model, AB stacking (brightest), CAB (medium), AAB (darkest), slip-AB (ignored); Rong and Kuiper's model, AAB stacking (brightest), slip-AB (second brightest), AB (second darkest), CAB (darkest). It is experimentally difficult to verify their models because STM cannot check the stacking of the topmost three layers of a superlattice. In order to clarify the controversy, we need a first-principles calculation of the local density of states on these kinds of stackings with a normal AB-stacked graphite bulk: ABABAB..., CABAB..., AABAB..., slip-ABAB.... This result will tell us the order of intensity with different kinds of stacking and thus different surface-atom sites, and it would be of tremendous aid to the understanding of the formation of superlattices.

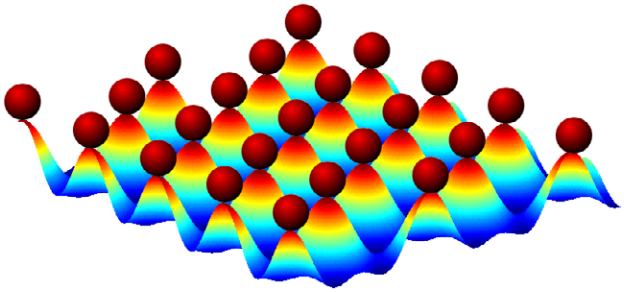

Figure 20. Possible application of superlattice in manipulating molecules or atoms in the form of an array by offering a template of adsorption sites where the periodicity can be predetermined. The balls represent adsorbed molecules or atoms, and the underlying template is the graphite superlattice.

3.2.3. Possible applications of superlattice structures. The Moiré phenomenon, the origin of a superlattice on graphite, has long been used in various applications, and it was first put into practical application by Lord Rayleigh in 1874 [81] for scrutinizing the fidelity of a replica of a diffraction grating. It is also a means for the metrologist and precision engineer for accurate measurement of tiny displacements. Moreover, the Moiré pattern gives a convenient method for the representation and solution of a variety of mathematical problems and for use the study of fields and flows in physics [59]. The work by Guo *et al* [82] and Liu *et al* [83] on nanometre Moiré fringes in STM show that by using the sample atomic lattice as the specimen grating and the STM scan lines as the reference grating, the Moiré pattern can offer a high sensitivity for surface deformation and defect measurement with nanometre spatial resolution. In view of these, it is conceivable that Moiré-induced superlattice structures have potential for precision measurement at the atomic scale. With the atomic lattices of the rotated graphene layers as the gratings, the resulting graphite superlattice consequently projects the small rotation angle between the two graphene layers onto the topmost layer in the form of a superperiodic hexagonal structure (superlattice) on a much larger scale. Given a scan range of a couple of micrometres for an STM, the rotation angle between two graphene layers can be detected with sensitivity down to a hundredth of a degree by imaging a superlattice with a periodicity of a few hundred nanometres.

Xhie *et al* [24] reported that the peaks (high electron density of states) of a superlattice are the preferential adsorption sites for both atoms and clusters. Together with the technique of manually creating superlattices by using STM tips discussed in section 2.7.6, this may present a way of preparing a template with any predetermined periodicity for adsorbing external atoms or molecules in the form of an array as illustrated in figure 20. This is potentially a more efficient way of manipulating atoms and molecules as it is a parallel process instead of in-series using scanning probe techniques.

Recently, atomically thin carbon films from a single layer to a few atomic layers were demonstrated to exhibit an electric field effect on applying a gate voltage, which may suggest graphite to be a suitable material for transistor applications, a potential candidate to get over the limits of performance improvement for the current electronics technology dominated by silicon [84, 85]. A Moiré rotation-induced superlattice

encompasses the electronic interaction between a few graphite layers; a STM tip scanning over a superlattice essentially resembles a transport measurement at every point of the superlattice. It has a similarity to the electrical measurements on atomically thin carbon films that Novoselov *et al* [84] suggested to be few-layer graphene (FLG) devices. The findings on the electronic interaction among graphene layers in superlattices observed using STM will be relevant to the development of FLG devices.

3.3. Conclusion

Graphite is one of the most studied substrates in STM, for its atomic flatness, chemical inertness, ease of preparation, and applicability as a weakly interacting substrate for experiments involving deposited species, be they chemical or biological objects. Graphite contains various kinds of defects, in particular superlattices, which are superperiodic structures with a hexagonal symmetry, which lead to ambiguity with the absorbed species.

A graphite superlattice, in its own right, is an intriguing phenomenon as its existence in STM images is in conflict with the general perception that an STM only probes the information at the topmost layer. There is constant research in the field concerning the origin and various properties of graphite superlattices. Despite the controversies, the Moiré rotation pattern assumption is generally accepted to be the major cause of the formation of a superlattice. Nevertheless, our understanding of superlattices is still rather limited; for instance, we are not totally clear about the reason for the anomalously large superlattice corrugation and its dependence on the tunnelling conditions.

The occurrence of a graphite superlattice is related to the dislocations caused by cleavage or crystal growth, and we do not have much control over this process. As such it is impossible to prepare a specific superlattice for experiments, which is part of the reason why research on this topic is restricted. Having said that, the situation is now changing. It is demonstrated that by using a STM tip, we can apply the tip–sample interaction to fold over a graphite layer to form a superlattice with a certain degree of control on the rotation angle and thus the resulting superlattice periodicity. On exposing graphite to chloroform, a high concentration of graphite superlattices is formed, which makes it easier to find a superlattice on a graphite surface to study.

As mentioned in sections 3.2.1 and 3.2.2, there are several research possibilities in the subject, both experimental and theoretical, along with the potential application of graphite superlattices in making a template for an array of adsorption sites and its relevance in developing new generation electronics devices, which render this subject a topic that deserves more research effort.

References

[1] Cotton F A and Wilkinson G 1988 *Advanced Inorganic Chemistry* Part 2, 5th edn (New York: Wiley)
[2] Albrecht T R, Dovek M M, Lang C A, Grutter P, Quate C F, Kuan S W, Frank C W and Pease R F W 1988 *J. Appl. Phys.* **64** 1178
[3] Arscott P G, Lee G, Bloomfield V A and Evans D F 1989 *Nature* **339** 484
[4] Coratger R, Claverie A, Ajustron F and Beauvillain J 1990 *Surf. Sci.* **227** 7
[5] Dunlap D D and Bustamante C 1989 *Nature* **342** 204
[6] Feng L, Hu C Z and Andrade J D 1988 *J. Colloid Interface Sci.* **126** 650
[7] Hara M, Iwakabe Y, Tochiji K, Sasabe H, Garito A F and Yamada A 1990 *Nature* **344** 228
[8] Horber J K H, Lang C A, Hansch T W, Heckl W M and Mohwald H 1988 *Chem. Phys. Lett.* **145** 151
[9] Lang C A, Horber J K H, Hansch T W, Heckl W M and Mohwald H 1988 *J. Vac. Sci. Technol.* A **6** 368
[10] Loo B H, Liu Z F and Fujishima A 1990 *Surf. Sci.* **227** 1
[11] Mizutan W, Shigeno M, Saito K, Watanabe K, Sugi M, Ono M and Kajimura K 1988 *Japan. J. Appl. Phys.* **27** 1803
[12] Smith D P E, Bryant A, Quate C F, Rabe J P, Gerber C and Swalen J D 1987 *Proc. Natl Acad. Sci. USA* **84** 969
[13] Smith D P E, Horber H, Gerber C and Binning G 1989 *Science* **245** 43
[14] Smith D P E, Kirk M D and Quate C F 1987 *J. Chem. Phys.* **86** 6034
[15] Wu X L and Lieber C M 1988 *J. Phys. Chem.* **92** 5556
[16] Albrecht T R, Mizes H A, Nogami J, Park S and Quate C F 1988 *Appl. Phys. Lett.* **52** 362
[17] Beyer H, Muller M and Schimmel Th 1999 *Appl. Phys.* A **68** 163
[18] Gan Y, Chu W and Qiao L 2003 *Surf. Sci.* **539** 120
[19] Garbarz J, Lacaze E, Faivre G, Gauthier S and Schott M 1992 *Phil. Mag.* A **65** 853
[20] Kuwabara M, Clarke D R and Smith D A 1990 *Appl. Phys. Lett.* **56** 2396
[21] Liu C Y, Chang H and Bard A J 1991 *Langmuir* **7** 1138
[22] Osing J and Shvets I V 1998 *Surf. Sci.* **417** 145
[23] Rong Z Y and Kuiper P 1993 *Phys. Rev.* B **48** 17427
[24] Xhie J, Sattler K, Ge M and Venkateswaran N 1993 *Phys. Rev.* B **47** 15835
[25] Hahn J R and Kang H 1999 *Phys. Rev.* B **60** 6007
[26] Kelly K F, Sarkar D, Hale G D, Oldenburg S J and Halas N J 1996 *Science* **273** 1371
[27] Kondo S, Lutwyche M and Wada Y 1994 *Japan. J. Appl. Phys.* **33** L1342
[28] Mizes H A and Foster J S 1989 *Science* **244** 559
[29] de Bont P W, Scholte P M L O, Hottenhuis M H J, van Kempen G M P, Kerssemakers J W and Tuinstra F 1994 *Appl. Surf. Sci.* **74** 73
[30] Porte L, de Villeneuve C H and Phaner M 1991 *J. Vac. Sci. Technol.* B **9** 1064
[31] Rabe J P, Sano M, Batchelder D and Kalatchev A A 1988 *J. Microscopy* **152** 573
[32] Shedd G M and Russell P E 1991 *J. Vac. Sci. Technol.* A **9** 1261
[33] Xhie J, Sattler K, Muller U, Venkateswaran N and Raina G 1991 *J. Vac. Sci. Technol.* B **9** 833
[34] Moncton D E, Axe J D and Disalvo F J 1977 *J. Phys. Rev. B: Condens. Matter* **16** 801
[35] Slough C G, McNairy W W, Coleman R V, Garnaes J, Prater C B and Hansma P K 1990 *Phys. Rev.* B **42** 9255
[36] Wu X L and Lieber C M 1989 *Science* **243** 1703
[37] Rong Z Y 1994 *Phys. Rev.* B **50** 1839
[38] Keller D, Bustamante C and Keller R W 1989 *Proc. Natl Acad. Sci. USA* **86** 5356
[39] Lee G, Arscott P G, Bloomfield V A and Evans D F 1989 *Science* **244** 475
[40] Beebe T P Jr, Wilson T E, Ogletree D F, Katz J E, Balhorn R, Salmeron M D and Siekhaus W J 1989 *Science* **243** 370
[41] Clemmer C R and Beebe T P Jr 1991 *Science* **251** 640
[42] Chang H and Bard A J 1991 *Langmuir* **7** 1143
[43] Pong W T and Durkan C 2005 *Japan. J. Appl. Phys., Part 1* **44** (7B) 5443
[44] Yang X, Bromm Ch, Geyer U and von Minnigerode G 1992 *Ann. Phys.* **1** 3
[45] Buckley J E, Wragg J L and White H W 1991 *J. Vac. Sci. Technol.* B **9** 1079
[46] Ouseph P J 1996 *Phys. Rev.* B **53** 9610

[47] Ouseph P J 2000 *Appl. Surf. Sci.* **165** 38
[48] Sun H, Shen Q, Jia J, Zhang Q and Xue Q 2003 *Surf. Sci.* **542** 94
[49] Feddes B, Kravchenko I I and Seiberling L E 1998 *Scanning* **20** 376
[50] Oden P I, Thundat T, Nagahara L A, Lindsay S M, Adams G B and Sankey O F 1991 *Surf. Sci. Lett.* **254** L454
[51] Song I K, Kitchin J R and Barteau M A 2002 *Proc. Natl Acad. Sci. USA* **99** (Suppl. 2) 6471
[52] Bernhardt T M, Kaiser B and Rademann K 1988 *Surf. Sci.* **408** 86
[53] Miyake K, Akutsu K, Yamada T, Hata K, Morita R, Yamashita M and Shigekawa H 1998 *Ultramicroscopy* **73** 185
[54] Pong W T and Durkan C 2005 *Japan. J. Appl. Phys., Part 1* **44** (7B) 5365
[55] Charlier J-C, Michenaud J-P and Gonze X 1992 *Phys. Rev.* B **46** 4531
[56] Lipson H and Stokes A R 1942 *Proc. R. Soc. Lond. Ser. A* **181** 101
[57] Sawamura M, Womelsdorf J F and Ermler W C 1991 *J. Phys. Chem.* **95** 8823
[58] Green T A and Weigle J 1948 *Helv. Phys. Acta* **21** 217
[59] Oster G 1968 *Endeavour* **27** 60
[60] Amidror I 1999 *The Theory of the Moiré Phenomenon* (Dordrecht: Kluwer)
[61] Kobayashi K 1996 *Phys. Rev.* B **53** 11091
[62] Charlier J-C, Michenaud J-P and Lambin Ph 1992 *Phys. Rev.* B **46** 4540
[63] Cee V J, Patrick D L and Beebe T P Jr 1995 *Surf. Sci.* **329** 141
[64] Hentschke R, Schurmann B and Rabe J 1992 *J. Chem. Phys.* **96** 6213
[65] Tersoff J and Hamann D R 1983 *Phys. Rev. Lett.* **50** 1998
[66] Wei Z, Xu C, Chen X and Xu K 2004 *Appl. Surf. Sci.* **228** 158
[67] Snyder S R, Gerberich W W and White H S 1993 *Phys. Rev.* B **47** 10823
[68] Gilman J J 1969 *Micromechanics of Flow in Solids* (New York: McGraw-Hill) chapter 5
[69] Soule D E and Nezbeda C W 1968 *J. Appl. Phys.* **39** 5122
[70] Ball S J, MacLeod J M and McLean A B 2005 Observation of solvent-induced superlatices of graphite suraces (in preparation)
[71] Dai G, Xie T, Cheng H and Ye H 2003 *J. Mater. Sci. Technol.* **19** 246
[72] Dalidchik F I, Grishin M V and Kovalevskii S A 2003 *Phys. Low-Dimens. Struct.* **3/4** 45
[73] Gwo S and Shih C K 1993 *Phys. Rev.* B **47** 13059
[74] Mamin H J, Ganz E, Abraham D W, Thomson R E and Clarke J 1986 *Phys. Rev.* B **34** 9015
[75] Soler J M, Baro A M, Garcia N and Rohrer H 1986 *Phys. Rev. Lett.* **57** 444
[76] Nysten B, Roux J-C, Flandrois S, Daulan C and Saadaoui H 1993 *Phys. Rev.* B **48** 12527
[77] Saadaoui H, Roux J-C, Flandrois S and Nysten B 1993 *Carbon* **31** 481
[78] Ganz E, Sattler K and Clarke J 1988 *Phys. Rev. Lett.* **60** 1856
[79] Muller U, Sattler K, Xhie J, Venkateswaran N and Raina G 1991 *J. Vac. Sci. Technol.* B **9** 829
[80] Patrick D L and Beebe T P Jr 1993 *Surf. Sci. Lett.* **297** L119
[81] Lord Rayleigh 1874 *Phil. Mag.* **47** 81
[82] Guo H M, Liu H W, Wang Y L, Gao H J, Shang H X, Liu Z W, Xie H M and Dai F L 2004 *Nanotechnology* **15** 991
[83] Liu Z W, Xie H M, Fang D N, Shang H X and Dai F L 2004 *J. Mater. Process Tech.* **148** 77
[84] Novoselov K S, Geim A K, Morozov S V, Jiang D, Zhang Y, Dubonos S V, Grigorieva I V and Firsov A A 2004 *Science* **306** 666
[85] Zhang Y, Small J P, Amori M E S and Kim P 2005 *Phys. Rev. Lett.* **94** 176803
[86] Lyding J W, Hubacek J S, Gammie G, Skala S and Brockenbrough R 1988 *J. Vac. Sci. Technol.* A **6** 363
[87] Elings V and Wudl F 1988 *J. Vac. Sci. Technol.* A **6** 412
[88] Womelsdorf J F and Ermler W C 1991 *J. Phys. Chem.* **95** 503
[89] Hashizume T, Kamiya I, Hasegawa Y, Sano N, Sakurai T and Pickering H W 1988 *J. Microscopy* **152** 347
[90] Digital Instruments 1988 *Phys. Today* **41** 129
[91] Markey L, Stievenard D, Devos A, Lannoo M, Demol F and de Backer M 1997 *Supramolecular Sci.* **4** 375
[92] Ball S J, Contant G E and McLean A B 2004 *Rev. Sci. Instrum.* **75** 5293
[93] Tanii T, Hara K, Ishibashi K, Ohta K and Ohdomari I 2000 *Appl. Surf. Sci.* **162–163** 662